

Volatile Organic Compound Detection Using Insect Odorant-Receptor Functionalised Field-Effect Transistors

by

Eddyn Oswald Perkins Treacher

A thesis submitted in fulfilment of the
requirements of the degree of
Doctor of Philosophy in Physics
School of Physical and Chemical Sciences
Te Herenga Waka - Victoria University of Wellington

Feb 2024



Table of contents

Acknowledgements	1
1. Verifying Non-Covalent Functionalisation of Carbon Nanotubes and Graphene	3
1.1. Introduction	3
1.2. Non-Covalent Bonding and π -Stacking	4
1.3. Attachment of 1-Pyrenebutanoic Acid N-Hydroxysuccinimide Ester	5
1.3.1. Comparing Attachment Methods	5
1.3.2. Examining 1-Pyrenebutanoic Acid N-Hydroxysuccinimide Ester Purity	9
1.3.3. Electrical Characterisation	10
1.4. Attachment of 1-Pyrenebutyric Acid	13
1.4.1. Comparing Attachment Methods	13
1.4.2. Raman Spectroscopy	13
1.4.3. Electrical Characterisation	15
1.5. Attachment of PEGlyated Pyrene-Based Linkers	17
1.5.1. Pyrene-NTA, Pyrene-Biotin and PEGylation	17
1.5.2. Fluorescence Characterisation with Pyrene-PEG-FITC	18
1.5.3. Electrical Characterisation with mPEG-Pyrene	20
1.6. Addressing Functionalisation Issues	23
1.6.1. Photoresist Contamination	23
1.6.2. Hydrophobicity of Carbon Nanotubes and Graphene	25
1.6.3. Substrate Interaction with Linker Molecules	26
1.6.4. “Coffee-Ring” Effect	28
1.7. Verifying Linker-OR Nanodisc Attachment	29
1.7.1. Functionalisation using PBASE	29
1.7.2. Functionalisation using Pyrene-PEG-NTA	31
1.8. Conclusions	33
Appendices	35
A. Python Code for Data Analysis	35
A.1. Code Repository	35
A.2. Atomic Force Microscope Histogram Analysis	35
A.3. Raman Spectroscopy Analysis	35

Table of contents

A.4. Field-Effect Transistor Analysis	35
---	----

Acknowledgements

69450

Rifat, Alex - vapour sensor
Erica Cassie - FET sensing setup
Rob Keyzers and Jennie Ramirez-Garcia - NMR spectra
Patricia Hunt - Computational chemistry

1. Verifying Non-Covalent Functionalisation of Carbon Nanotubes and Graphene

310589

1.1. Introduction

In previous chapters, I have discussed methods of fabricating carbon nanotube and graphene devices and then shown that they are sensitive to environmental changes in a saline solution. However, for specific sensing, the devices require (bio)chemical functionalisation. Instead of responding to stimuli themselves, the sensing signal is picked up by attached receptors. The devices then act as passive transducers for the received signal. Receptors previously used with carbon nanotube and graphene devices include aptamers [1]–[6] and a range of proteins [7]–[10], including animal odorant receptors [11]–[16]. A common approach to attaching receptors to the transducer involves the use of a linker molecule to tether the receptor to the transducer. Verifying that this linker molecule is bridging between the transducer and the receptor element is important for a complete understanding of the behaviour of these sensors. This verification involves providing evidence for effective attachment of linker molecule to the transducing device channel, then showing successful tethering of odorant receptors and other biomolecules to the attached linker molecule.

This chapter therefore takes some time exploring the following selection of available linker molecules for specific biosensing: 1-Pyrenebutanoic Acid N-Hydroxysuccinimide Ester (PBASE), 1-Pyrenebutyric Acid (PBA), Pyrene-PEG-NTA (PPN) and Pyrene-PEG-Biotin (PPB). The linker molecules used are discussed in detail, and numerous hurdles to successful functionalisation via linker molecules are identified and addressed. Next, it looks at verifying that the odorant receptor proteins of interest have specifically attached to these linker molecules. The experimental parameters used for both the attachment of linker molecules and receptor proteins are also varied, and the impact of these variations on successful functionalisation is investigated via Raman spectroscopy, fluorescence microscopy and electrical characterisation.

1. Verifying Non-Covalent Functionalisation of Carbon Nanotubes and Graphene

1.2. Non-Covalent Bonding and π -Stacking

Linker molecules may be attached via covalent or non-covalent bonding to carbon nanomaterials, such as carbon nanotubes and graphene. Covalent bonding is stronger than non-covalent bonding, and therefore gives a more permanent attachment between linker molecules and the transducer. However, non-covalent bonding has the advantage of having less of an impact on the structure of a nanomaterial than covalent bonding, meaning non-covalent bonding is less likely to negatively affect the electrical properties of the transducer [1], [5], [10], [17], [18]. For example, one group found covalent bonding of diazonium linker caused a $\sim 50\%$ drop in graphene channel mobility [7]. In comparison, only a $\sim 5\%$ drop in mobility was seen for attachment of a mixture of linkers containing pyrene to a graphene channel via non-covalent π stacking [19].

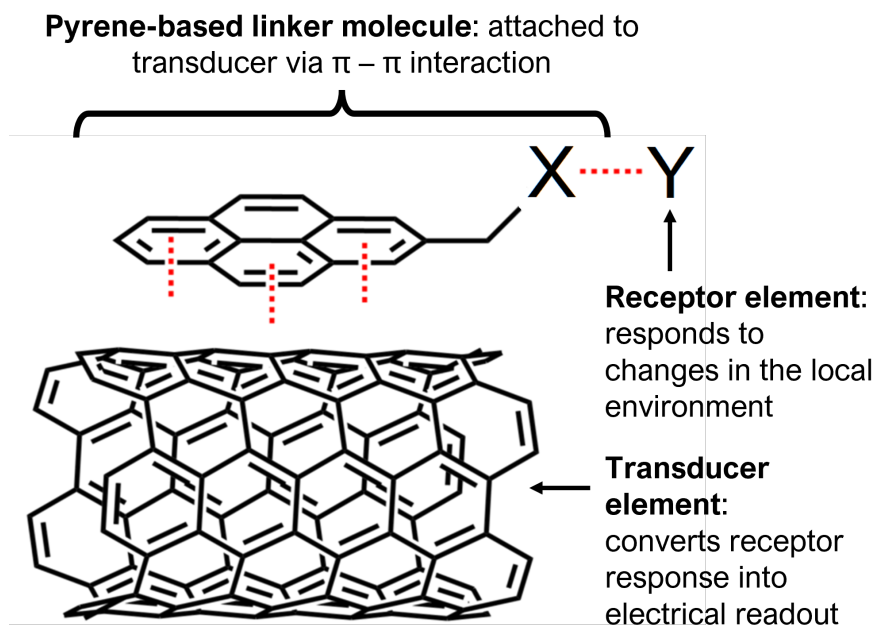


Figure 1.1.: Attachment of pyrene-based linker molecule pyrene-X and receptor Y to a carbon nanotube, representing the transducer element of a field-effect transistor. Source: Adapted from [20].

π -stacking or $\pi - \pi$ interaction is often used to describe a type of non-covalent bonding which occurs due to dispersion forces between unsaturated polycyclic molecules [21]. It has been argued that this label is unhelpfully specific and a misrepresentation of what can be simply classed as a type of Van Der Waals bonding [21], [22]. However, as the use of the term is widespread in the literature, it is also used here for the sake of clarity. Carbon nanotubes and graphene consist of a network of carbon atoms attached to each other by sp^2 hybrid orbitals in a polycyclic structure. They are therefore able to strongly interact with linker molecules with aromatic moieties, such as pyrene [5], [21],

1.3. Attachment of 1-Pyrenebutanoic Acid N-Hydroxysuccinimide Ester

[23]. Figure 1.1 is a visual demonstration of the relationship between the pyrene-based linker molecule with the transducer and receptor elements. A wide range of pyrene-based linker molecules have been used for non-covalent modification of carbon nanotubes and graphene [24]. π -stacking with pyrene is the bonding mechanism underlying all the functionalisation processes in this thesis.

1.3. Attachment of 1-Pyrenebutanoic Acid N-Hydroxysuccinimide Ester

1.3.1. Comparing Attachment Methods

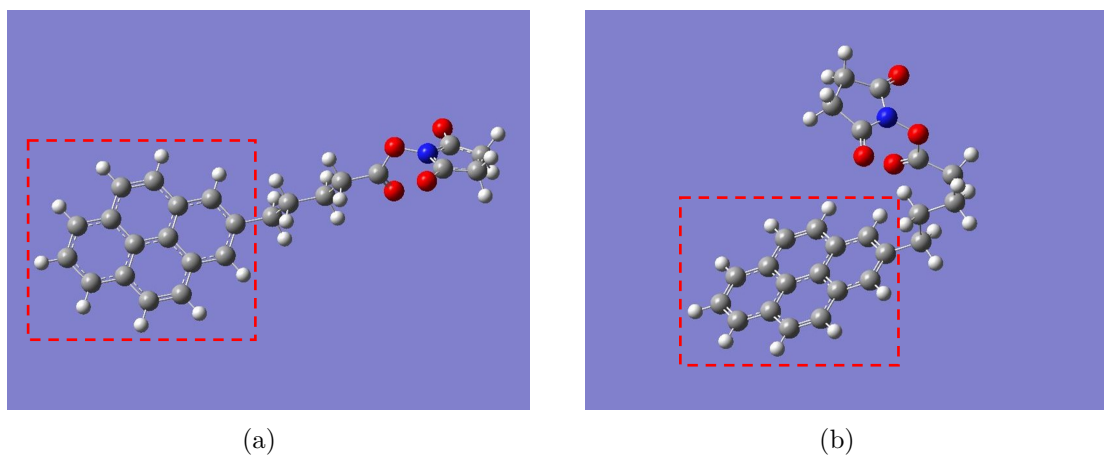


Figure 1.2.: Two conformations of PBASE molecule with geometry optimised via *ab initio* calculations performed with Gaussian 16 software [25]. White balls correspond to hydrogen, grey to carbon, red to oxygen and blue to nitrogen. The pyrene moiety is highlighted in the image with a red dashed outline.

1-pyrenebutanoic acid N-hydroxysuccinimide ester (also known commercially and in the literature both as 1-pyrenebutyric acid N-hydroxysuccinimide ester and 1-pyrenebutanoic acid succinimidyl ester; acronyms include PBASE, PBSE, PyBASE, PASE, PYSE, PSE, Pyr-NHS and PANHS) is a aromatic molecule commonly used for tethering biomolecules to the carbon rings of graphene and carbon nanotubes. Using computational modelling, two locally stable molecular conformations were found to exist, a straight (Figure 1.2a) and bent (Figure 1.2b) structure. The conformation in Figure 1.2a has a Hartree-Fock energy of -3427728.67 kJ/mol, while the conformation in Figure 1.2b has a Hartree-Fock energy of -3427729.66 kJ/mol. The difference between computed Hartree-Fock energies is 1.0 kJ/mol, small enough that the existence of both molecular conformations is physically feasible. Similar straight and bent structures have previously been modelled for PBASE attached to graphene [26].

1. Verifying Non-Covalent Functionalisation of Carbon Nanotubes and Graphene

Table 1.1.: Comparison of PBASE functionalisation processes used for immobilisation of proteins and aptamers onto carbon nanotubes and graphene. Experimentally optimised variables are marked with a star (*). Blank entries indicate there was no mention of the parameter in a particular paper.

Solvent	Channel	Conc. (mM)	Incubation type	Time (hr)	Rinse steps	References
DMF	CNT	5	Immersed	1	PBS	Maehashi, 2007. [27]
		6	Immersed	1	DMF, PBS	García-Aljaro, 2010. [28]
		6	Immersed	1	DMF	Chen, 2001. [29]
		6	Immersed	1	DMF	Cella, 2010. [30]
		6	Immersed	1	DMF	Das, 2011. [31]
		6	-	2	DMF	Besteman, 2003. [32]
	Graphene	-	-	2	DMF	Tsang, 2019. [33]
		-	-	20	-	Wiedman, 2017. [34]
		0.2	Immersed	20	DMF, IPA, DI water	Gao, 2018. [35]
		1	Dropcast	6	DMF, IPA, DI water	Nekrasov, 2021. [4]
		5	Immersed	1	DMF, DI water	Hwang, 2016. [36]
		5*	Immersed	3*	DMF	Hao, 2020. [37]
		5	Immersed	4*	DMF, DI water	Mishyn, 2022. [5]
		6	Dropcast	2	DMF, DI water	Nur Nasufiya, 2020. [38]
		10	Dropcast	2	DMF, DI water	Campos, 2019. [39]
	2-Methoxyethanol	10	Immersed	2	DMF, PBS	Kuscu, 2020. [40]
		10	Immersed	1	DMF	Xu, 2017. [41]
		10	Immersed	12	DMF, EtOH, DI water	Khan, 2020. [42]
		50	Immersed	4*	MeOH	Wang, 2020. [10]
		1	Immersed	1	DI water	Ono, 2020. [43]
Methanol	CNT	1	Immersed	1	MeOH, DI water	Zheng, 2016. [44]
		1	Immersed	2	MeOH	Kim, 2009. [45]
	Graphene	100	Dropcast	1	DI water	Yoo, 2022. [16]
		5	Immersed	2	-	Sethi, 2020. [46]
DMSO	CNT	5	Immersed	1	MeOH, PBS	Ohno, 2010. [47]
		10	-	1	DI water	Lopez, 2015. [48]
		10	Immersed	1	PBS	Strack, 2013. [49]

1.3. Attachment of 1-Pyrenebutanoic Acid N-Hydroxysuccinimide Ester

The pyrene moiety, highlighted with a red dashed outline in Figure 1.2a-b, non-covalently bonds to the carbon rings of the carbon nanotube and graphene surface. The N-hydroxysuccinimide (NHS) ester group, seen on the right-hand side of Figure 1.2, is highly reactive with amine groups. It can undergo a nucleophilic substitution reaction with amines attached to proteins or aptamers, tethering these biomolecules via an amide or imide bond [5], [23], [29], [50].

The non-covalent functionalisation of proteins onto a single-walled carbon nanotube using PBASE was first reported by Chen *et al.* in 2001 [29]. Two successful methods for protein functionalisation and immobilisation were reported, with the only differences being the solvent used to dissolve the PBASE powder (DMF, methanol) and the final concentration of the resulting solutions (6 mM, 1 mM respectively). PBASE powder appears to dissolve poorly in methanol at higher concentrations, which might explain the use of different concentrations of PBASE in each solvent. An extensive comparison of methods used in the literature for PBASE functionalisation of carbon nanotube and graphene devices with aptamers and proteins is given in Table 1.1. Several listed works directly cite Chen *et al.* when discussing functionalisation with PBASE [30], [32], [39], [44], [47]. The other works listed do not explicitly reference Chen *et al.* in their methodology; however, the frequency of methods detailing the use of 6 mM PBASE in dimethylformamide (DMF) and 1 mM PBASE in methanol indicate that these processes are largely copying the process used by Chen *et al.*.

However, it is also apparent from Table 1.1 that there is a large degree of variation in the methods used for PBASE functionalisation. Various electrical characterisation, microscopy and spectroscopy techniques have been used to demonstrate successful functionalisation. Until recently, there has been little justification provided for the selection of variables used in the functionalisation procedure (e.g. length of time submerged in solvent containing PBASE), despite the wide-ranging use of this process in the literature [10], [51], [52]. This is surprising, given that the sensitivity of functionalised devices is considered to be closely related to the density of surface functionalisation [50], [53], [54]. Furthermore, a detailed investigation of PBASE functionalisation process variables has only been undertaken for graphene-based devices [5], [10], [37], [52].

Zhen *et al.* [52], Wang *et al.* [10] and Mishyn *et al.* [5] have all claimed that carefully tuning the surface concentration of PBASE is required to avoid multilayer coverage of the graphene surface, as this negatively impacts sensing. Mishyn *et al.* [5] used cyclic voltammetry to demonstrate that less receptor attachment to the graphene surface occurs when multiple layers of PBASE are present. However, none of these groups have presented analyte sensing results from their functionalised graphene devices. In contrast, Hao *et al.* [37] found that maximising the PBASE surface coverage of a channel resulted in more sensitive aptameric sensing, thereby reaching the opposite conclusion. The inconsistency in these recent findings mean more work is needed to understand the PBASE functionalisation process to achieve optimal biosensor sensitivity. It may also be the case that a specific functionalisation process is required for optimal sensitivity with the use of a specific type of receptor.

1. Verifying Non-Covalent Functionalisation of Carbon Nanotubes and Graphene

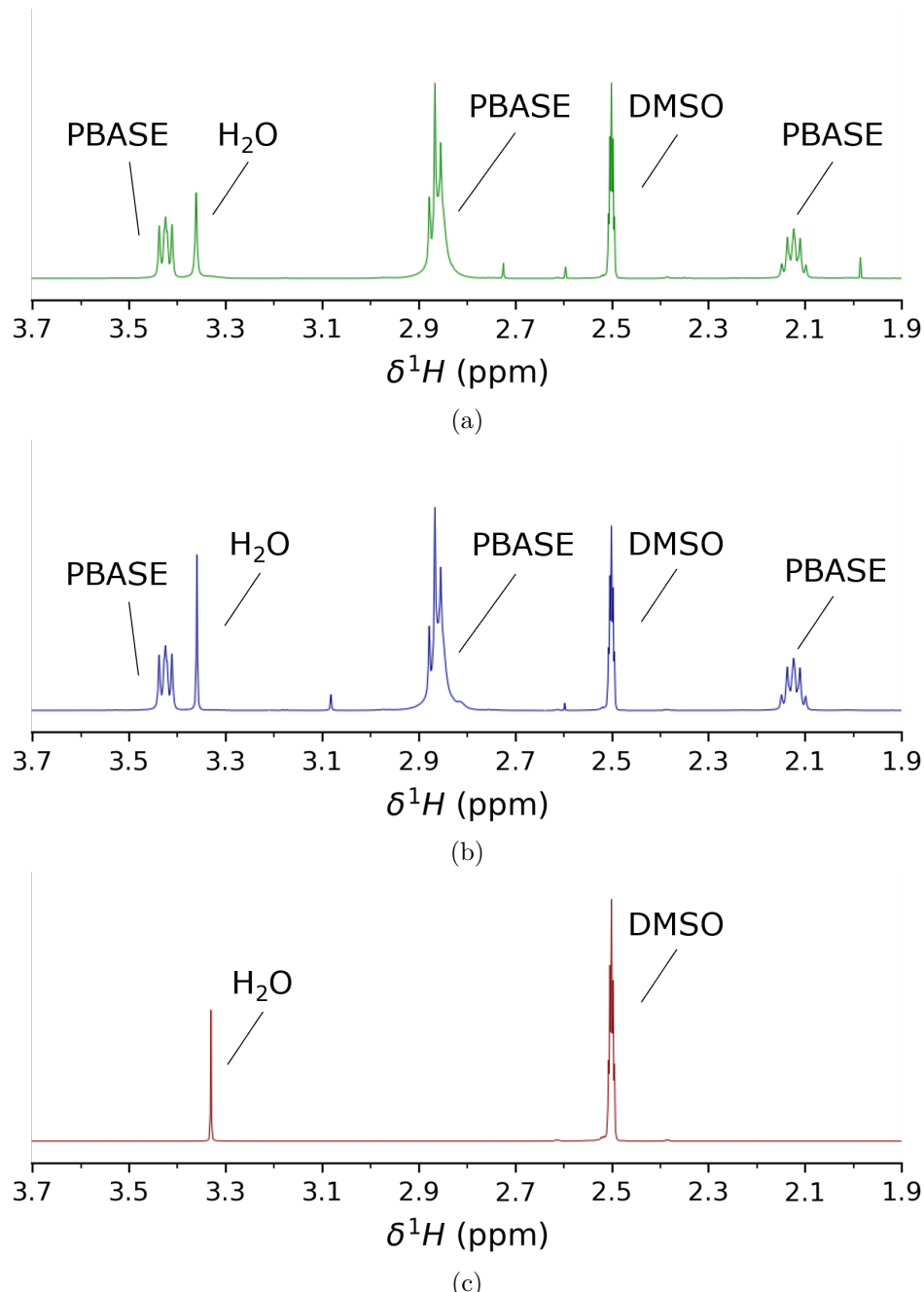


Figure 1.3.: ^1H Nuclear Magnetic Resonance (NMR) spectra, performed with DMSO-d₆ used as the NMR solvent. (a) and (b) show NMR spectrum for commercially purchased PBASE, from Sigma-Aldrich and Setareh Biotech respectively, while (c) shows the blank spectrum taken with only DMSO-d₆ present (spectra taken by Jennie Ramirez-Garcia, School of Chemical and Physical Sciences, Te Herenga Waka - Victoria University of Wellington). Unlabelled peaks correspond to sample impurities.

1.3. Attachment of 1-Pyrenebutanoic Acid N-Hydroxysuccinimide Ester

Once fastened to a bioreceptor via an amide or imide bond, the attachment to the linker molecule is not easily broken. However, prior to use in functionalisation processes, the NHS ester may react with any water present (hydrolysis). This reaction converts PBASE to 1-pyrenebutyric acid (PBA), leaving it unavailable to react further with amine groups [5], [50], [55]. If the amine group functionalisation is performed within a ~ 1 hour period, with a high concentration of bioreceptor used at close to neutral pH, competing hydrolysis should not have a significantly adverse impact on the functionalisation process [50]. However, if PBASE is exposed to water during storage over a significant length of time, the presence of 1-Ethyl-3-(3-dimethylaminopropyl)carbodiimide (EDC) can be used to restore the NHS ester and enable the substitution reaction to take place (see discussion of PBA/EDC in Section 1.4).

1.3.2. Examining 1-Pyrenebutanoic Acid N-Hydroxysuccinimide Ester Purity

I purchased PBASE from two suppliers, Sigma-Aldrich and Setareh Biotech. Sigma recommended DMF and methanol as suitable solvents for dissolving PBASE, alongside chloroform and dimethyl sulfoxide (DMSO). Setareh Biotech indicated methanol can be used for dissolving PBASE. The two suppliers had conflicting information for suitable storage of PBASE, with Sigma recommending room temperature storage while Setareh Biotech recommends storage of -5 to -30°C and protection from light and moisture. I used nuclear magnetic resonance (NMR) spectroscopy to verify the purity of PBASE from various suppliers. As water can react with PBASE to form unwanted byproducts, it appears that protection from moisture is particularly important. A particular emphasis was placed on detecting water presence in the received samples, considering the long travel time of the PBASE with uncertain storage conditions.

Figure 1.3 compares the shapes of hydrogen NMR spectra of PBASE from each supplier when dissolved in deuterated DMSO, alongside a blank deuterated DMSO spectrum. Both PBASE samples possessed characteristic chemical shift features between 2.1 – 2.2 ppm, 2.8 – 2.9 ppm, and 3.4 – 3.5 ppm. These chemical shifts roughly correspond to those seen in previous NMR spectra for PBASE [56]. The feature at 2.50 ppm represents the deuterated DMSO solvent, while the single peak between 3.3 – 3.4 ppm represents the water present in the sample. By comparing the area of these peaks, a rough estimate of the amount of water originally present in the PBASE sample can be obtained. The $\text{H}_2\text{O:DMSO}$ ratio is 1:7 in the blank spectrum, but $\sim 1:3$ in the provided samples, possibly indicating the introduction of water to the PBASE during production or storage. However, DMSO is strongly hygroscopic and slight differences in DMSO storage time, as well as differences in humidity during sample preparation, may have had a significant impact on this result [57]. Other impurities are also seen on both PBASE spectra, though their small size indicates they make up only a small percentage of each sample. Strack *et al.* [49] recommend leaving frozen PBASE at room

1. Verifying Non-Covalent Functionalisation of Carbon Nanotubes and Graphene

temperature for 15 minutes before exposing it to air to prevent condensation near the PBASE, as this can cause unnecessary H_2O contamination.

1.3.3. Electrical Characterisation

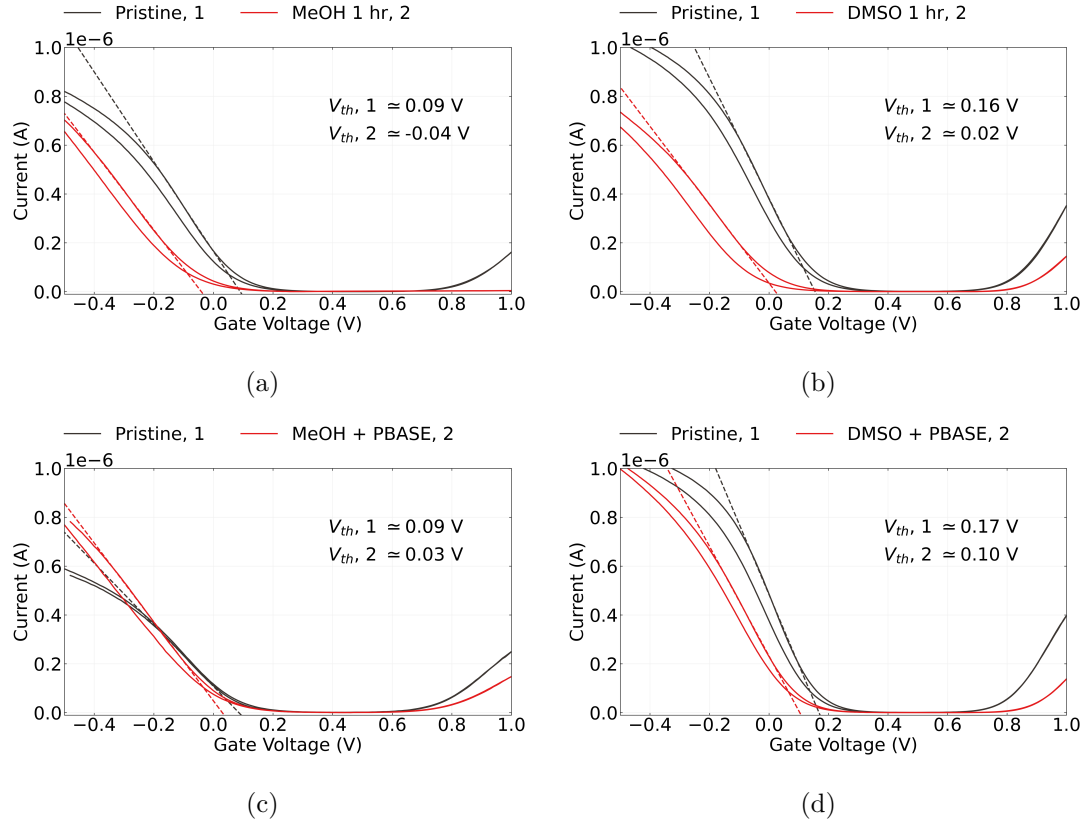


Figure 1.4.: The electrical transfer characteristics of carbon nanotube transistors ($V_{ds} = 100$ mV) before and after being submerged in methanol (a) or dimethyl sulfoxide (b) for one hour and subsequently rinsed with deionised water. The change in characteristics of similar transistor channels after being submerged in these same solvents containing 1 mM PBASE for one hour and then rinsed are shown in (c) and (d) respectively. Average threshold voltages for each transfer characteristic curve are also shown (taking the average of forward and reverse sweep values).

The electrical characteristics of the carbon nanotube or graphene transistor are often used to verify successful functionalisation and make a statement about the effect of chemical modification on the channel. However, this verification usually does not account for the effect of the solvent on the transistor channel. Figure 1.4a and Figure 1.4b show that by exposing a steam-deposited carbon nanotube network channel to solvents

1.3. Attachment of 1-Pyrenebutanoic Acid N-Hydroxysuccinimide Ester

commonly used in PBASE functionalisation processes (Table 1.1), such as methanol (MeOH) or dimethyl sulfoxide (DMSO), a significant negative shift in channel threshold voltage occurs even after thorough rinsing with deionised water. Besteman *et al.* reported observing a similar effect from prolonged exposure of a single carbon nanotube to dimethylformamide (DMF) [32]. It appears that the carbon nanotubes have adsorbed solvent which persists even after device cleaning. From the shape of the change in the transfer curve, it seems the residual polar solvent molecules capacitively gate the channel [58], [59].

Furthermore, using the same characterisation process as in this work, Murugathas *et al.* [13] showed that π -stacking of PBASE onto a solvent-deposited carbon nanotube network had little effect on channel threshold voltage, implying the presence of PBASE had not significantly influenced channel gating [13]. However, they did observe a slight increase in channel conductance after PBASE functionalisation. In Figure 1.4, a slight increase in channel conductance post-functionalisation is observed for both Figure 1.4c and Figure 1.4d when compared to the solvent-only case in Figure 1.4a and Figure 1.4b. This result implies that the presence of PBASE molecules increases channel mobility and therefore conductance [59].

Capacitive gating results from dense coverage of adsorbed molecules on the carbon nanotube surface which have a low permittivity relative to the surrounding electrolyte [59]. The relative permittivity of MeOH and DMSO are ~ 33 [60] and ~ 47 [61] respectively, which are both much lower than the relative permittivity of phosphate buffer saline, ~ 80 [3]. From Figure 1.4a and Figure 1.4b, the threshold shift values found resulting from exposure to each solvent, taking the average of forward and reverse sweep values from a single device, were $\Delta V = -0.15 \pm 0.02$ V and $\Delta V = -0.15 \pm 0.01$ V for MeOH and DMSO respectively. The average threshold shift value for a second device exposed to MeOH was $\Delta V = -0.16 \pm 0.02$ V, indicating that this threshold shift result is reproducible. The threshold voltage shifts in Figure 1.4c and Figure 1.4d from the pristine are small compared with the devices exposed to solvent only - this is likely due to the effect of increased conductance from the PBASE competing with the gating effect from the residual solvent.

The absorption of organic solvent by the carbon nanotube network has unknown but potentially negative implications for biosensor functionalisation. Use of organic solvents in functionalisation can also attack the encapsulation layer of devices, promoting gate current leakage. In light of these issues, recent work has begun to explore alternative aqueous-based methods for functionalisation of biosensors [1]. The discussion here also illustrates the importance of considering each substance used when electrical characterising a device to verify if functionalisation has worked. The qualitative presence of a change in characteristics (or lack of one) over the full process is not sufficient to make conclusive remarks regarding successful functionalisation. A full set of electrical control measurements are required for an understanding of electronic changes occurring during the functionalisation process, in the manner of Besteman *et al.* [32].

1. Verifying Non-Covalent Functionalisation of Carbon Nanotubes and Graphene

Table 1.2.: Comparison of 1-pyrenebutyric acid (PBA) functionalisation processes used for immobilisation of proteins, enzymes and aptamers onto carbon nanotubes and graphene. 1-ethyl-3-(3-dimethylaminopropyl) carbodiimide hydrochloride (EDC) and NHS were co-mingled in buffer/electrolyte solution or DI water in each process - some papers used N-hydroxysulfosuccinimide instead of N-hydroxysuccinimide, and both compounds are abbreviated as NHS in this table for simplicity. Device exposure times to each solution are shown next to the solution concentration. Blank entries indicate there was no mention of the parameter in a particular paper. [†]PEG or PEG pyrene were used to reduce non-specific binding. ^{††}Several pyrene-based linkers were compared and PBA gave an optimal functionalisation result.

Solvent	Channel	PBA (mM)	Time (hr)	EDC (mM)	NHS (mM)	Time (min)	References
DMF	Graphene	0.6	1	-	-	120	Gao, 2016 [†] . [62]
		5	2	2	5	30	Mishyn, 2022. [5]
	CNT	100	3	200	-	30	Min, 2012. [63]
	Graphene, CNT	7.6	2	8	20	120	Xu, 2014. [64]
DI water	CNT	-	-	32	12	Overnight	Pacios, 2012 [†] . [65]
Ethanol	CNT	1	1	100	100	20	Filipiak, 2018 [†] . [66]
Acetonitrile	Graphene	1	1	400	100	60	Tong, 2020 ^{††} . [9]
Borax	CNT	2	24	2.5	-	1080	Liu, 2011 [†] . [67]
DMSO	Graphene	5	1	50	50	90	Fenzl, 2017. [68]

1.4. Attachment of 1-Pyrenebutyric Acid

1.4.1. Comparing Attachment Methods

Another linker molecule that can be used to attach receptor molecules to a carbon nanotube or graphene channel is 1-pyrenebutyric acid (PBA or PyBA). As with PBASE, the pyrene group of PBA has a π interaction with the carbon rings of the channel surface. It is possible to react PBA with 1-ethyl-3-(3-dimethylaminopropyl) carbodiimide hydrochloride (EDC or EDAC) to form an *O*-acylisourea intermediate, which can then react with an amine group on a biomolecule and form an amide bond [69], [70]. The water solubility of EDC means that, unlike PBASE, it is possible to functionalise with EDC dissolved in water rather than in an organic solvent. However, like PBASE, EDC and the *O*-acylisourea intermediate are prone to hydrolysis, especially in acidic conditions. Therefore, like PBASE, it should be stored at -20°C , and warmed to room temperature to prevent condensation build-up, since exposure to condensation will hydrolyse the reagent [70]. Furthermore, by adding N-Hydroxysuccinimide (NHS) or N-hydroxysulfosuccinimide (sulfo-NHS) to the reaction vessel, PBASE is formed as an active intermediate, which is less prone to hydrolysis and increases the PBA/EDC reaction yield [69]–[71].

A full comparison of functionalisation procedures used for linking carbon nanotube and graphene devices to aptamers and proteins with PBA is given in Table 1.2. To the best of my knowledge, this table is as complete a summary as possible of 1-pyrenebutyric acid functionalisation processes for carbon nanotube and graphene field-effect transistor biochemical sensors. By comparing Table 1.1 and Table 1.2, it is clear that PBASE is more widely used for non-covalent functionalisation than PBA/EDC. As was the case for PBASE, there are a wide range of process variables used for the functionalisation process, with little justification used for variables chosen. Also notable is the frequent use of polyethylene glycol (PEG) or pyrene-PEG for prevention of non-specific binding (NSB). Non-specific binding is discussed further in [?@sec-non-specific-binding](#). Despite being less widely used, Mishyn *et al.* [5] state a preference for the use of PBA/EDC over PBASE, as they found it was less prone to hydrolysis and gave a larger reaction yield when binding ferrocene to graphene. A potential downside of using PBA/EDC for protein immobilisation is that EDC has numerous ways of interacting with proteins, and not all of these are necessarily desirable; furthermore, the addition of NHS may also cause other issues, such as precipitation of the reaction compound [70]. The greater range of process variables involved in the functionalisation also adds to the complexity of reproducing past results.

1.4.2. Raman Spectroscopy

Raman spectroscopy was used to verify the attachment of PBA to a carbon nanotube network film with a silicon dioxide substrate in the manner outlined in [?@sec-raman-](#)

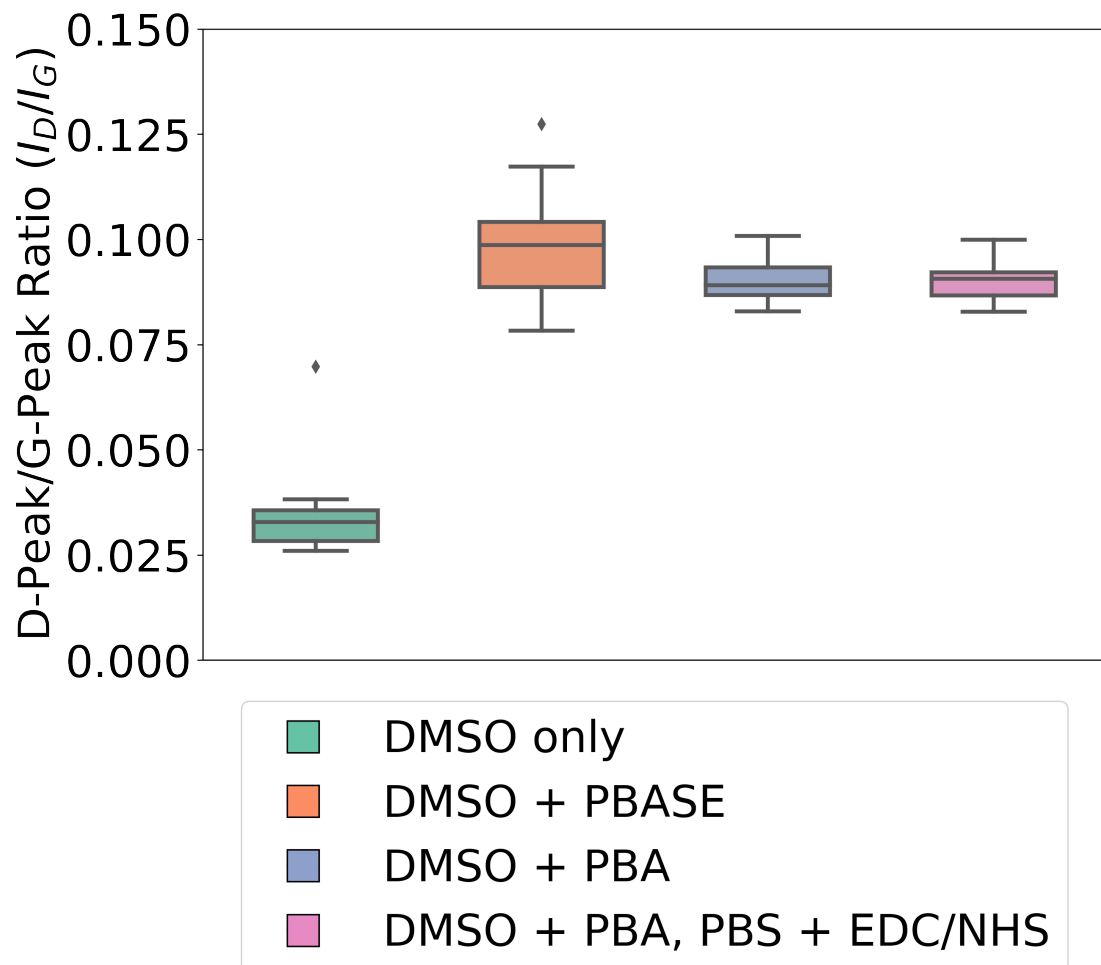


Figure 1.5.: This box plot shows the distribution of D-band peak to G⁺-band peak ratio, I_D/I_G , across nine locations for a selection of chemically-modified carbon nanotube films. The D-band and G-band intensities for all samples were first normalised to the intensity peak corresponding to the silicon dioxide substrate.

1.4. Attachment of 1-Pyrenebutyric Acid

characterisation. As highly-bundled devices were found to have less defects present prior to modification, as discussed in ?@sec-pristine-raman, solvent-deposited films were used for the verification of pyrene attachment to prevent the initial presence of defects influencing the analysis. Droplets of DMSO solution were placed on three (solvent-deposited) carbon nanotube films taken from the same wafer. The DMSO solution on one film contained 5 mM PBA, the solution on another film contained 5 mM PBASE, and the DMSO on the final film contained no linker molecule. After incubation for 1 hour, films were rinsed for 15 s with DMSO, then for 15 s with IPA to remove excess DMSO while avoiding hydrolysis of the PBASE. After the first set of Raman spectra was taken, the film initially exposed to PBA was further exposed to a solution of 20 mM EDC and 40 mM NHS in 1XPBS electrolyte for 30 minutes, and a second set of Raman spectra was taken for this film. As in ?@sec-pristine-raman, two spectra taken at each position were processed according to Section A.3, and the silicon dioxide reference peak measured in the wavenumber range $100\text{ cm}^{-1} - 650\text{ cm}^{-1}$ was used to normalise the D-band and G-band peaks from the wavenumber range $1300\text{ cm}^{-1} - 1650\text{ cm}^{-1}$. The ratio between the average intensity of the D-peak and the G^+ -peak at each position was calculated, and the distribution of ratio values corresponding to each modified film is shown in Figure 1.5.

There is a $\sim 3\times$ increase in the intensity ratio I_D/I_G for both the films modified with PBASE and PBA compared to the film which was only exposed to DMSO. Previous works have found that a change in the intensity ratio indicates successful π -stacking on the carbon nanotube surface, as it indicates surface modification of the carbon nanotubes has occurred [72], [73]. Wei *et al.* [72] found functionalisation with PBASE altered the ratio by a factor of $\sim 1.5\times$, while Lan *et al.* [73] found that functionalisation with PBA altered the ratio by a factor of $\sim 0.8\times$. The reason for the large difference between results is not immediately clear, but may result from the significant differences in the pristine composition and morphology of carbon nanotube networks used in each publication, and differences in the functionalisation method used. Across all scan locations in ?@fig-raman-comparison, the value found for I_D/I_G is consistently ~ 0.095 for both PBA and PBASE. Furthermore, subsequent Raman measurements of the PBA-modified film after further functionalisation with EDC/NHS do not show a significant change in I_D/I_G . These results indicate that presence of the NHS ester has little effect on the Raman shift. It should be clarified that Raman spectroscopy cannot be used to distinguish between the presence of PBA and PBASE on the device surface. However, it is clear that functionalisation of the carbon nanotube network with both the PBA and PBASE has led to measurable π -stacking between the network and the pyrene group attached to each compound.

1.4.3. Electrical Characterisation

Figure 1.6 shows the transfer characteristics of a carbon nanotube transistor channel at various stages of a PBA/EDC functionalisation, where a excess of N-hydroxysuccinimide

1. Verifying Non-Covalent Functionalisation of Carbon Nanotubes and Graphene

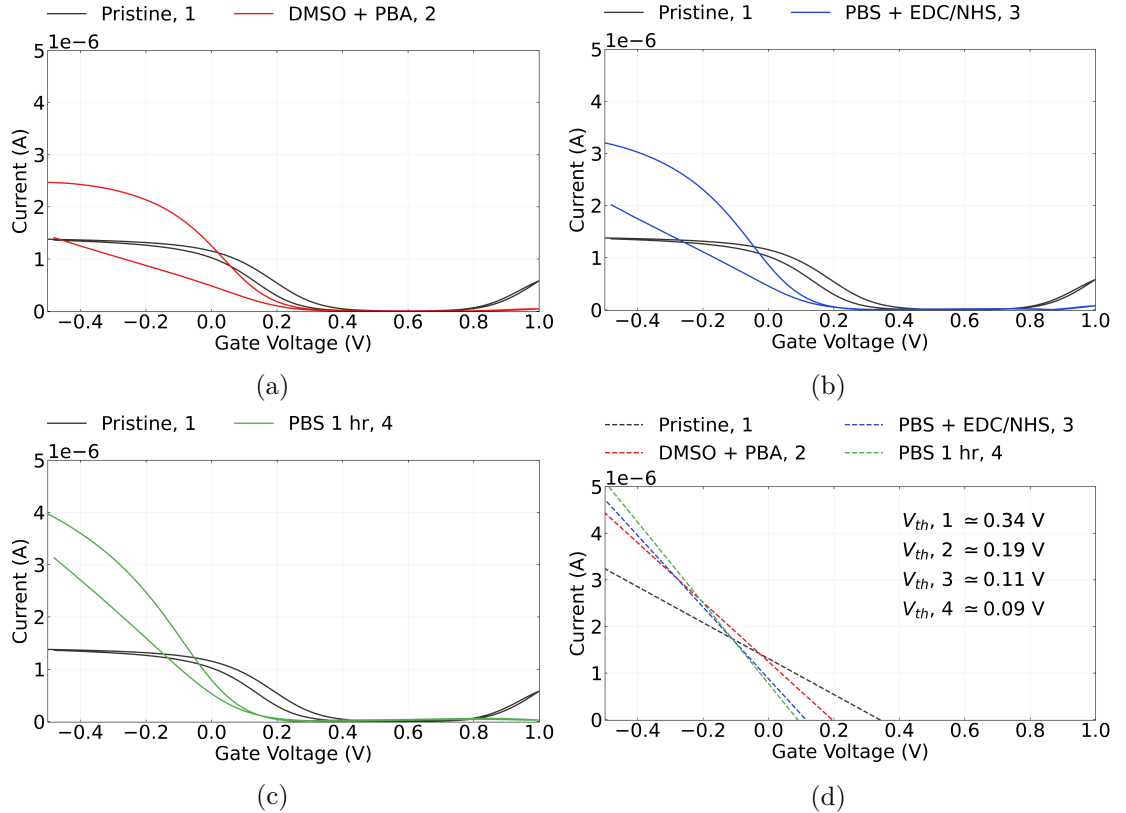


Figure 1.6.: Electrical transfer characteristics of a carbon nanotube transistor before functionalisation alongside the transfer characteristics (a) after being submerged in DMSO containing 5 mM PBA for 1 hour in red, (b) after being submerged in 1XPBS containing 20 mM EDC and 40 mM NHS for 30 min in blue, and (c) after being submerged in fresh 1XPBS for 1 hour in green. The linear fits to each characteristic curve are shown in (d) as dashed lines, alongside the threshold voltages calculated by finding the intercept of each fit.

1.5. Attachment of PEGlyated Pyrene-Based Linkers

(NHS) was added alongside EDC. A solvent-deposited carbon nanotube film was used for the device. The PBA was dissolved in DMSO, and the device channels were exposed to this solution for 1 hour. The electrical change resulting from PBA exposure is shown in Figure 1.6a. The threshold shift with the addition of 5 mM PBA in DMSO for 1 hour is equivalent to the shift seen when only DMSO is added, $\Delta V = -0.15$ V. The lack of a significant threshold shift directly attributable to the PBA is a result of pyrene having a neutral charge state; any contributions from the charged carboxyl group are screened from the carbon nanotube sidewalls by surrounding water molecules [74]. However, as in the case of the addition of PBASE, there also appears to be an increase in hole mobility, which may be due to the pyrene groups increasing connectivity within the carbon nanotube network [13].

Subsequently, the device was rinsed with 1XPBS and exposed to 20 mM EDC and 40 mM NHS in 1XPBS electrolyte for 30 minutes. Figure 1.6b shows the change resulting from subsequent EDC/NHS exposure. When EDC/NHS is added, a threshold shift of $\Delta V \sim -0.08$ V was observed on multiple channels. The exposure to EDC/NHS negatively shifts the transfer characteristic curve, most likely due to the PBA present reacting to form positively-charged *O*-acylisourea esters and negatively gating the attached carbon nanotube network [59], [70]. Figure 1.6c shows that this shift is not significantly affected by further exposure of the channel to PBS. This indicates that hydrolysis over the course of one hour is insufficient to hydrolyse a significant proportion of the *O*-acylisourea back to PBA, as PBA is charge neutral. We therefore expect that a significant amount of *O*-acylisourea remains active within this time period and available for reaction with biomolecule amine groups.

1.5. Attachment of PEGlyated Pyrene-Based Linkers

1.5.1. Pyrene-NTA, Pyrene-Biotin and PEGylation

Through chemical coupling/conjugation, it is possible to replace the NHS ester group on PBASE with other groups that can undergo binding reactions with proteins. Unlike PBASE, these groups do not suffer the drawback of being readily hydrolysed. For example, PBASE can be modified with Na,Na -Bis(carboxymethyl)-L-lysine hydrate (also known as N-(5-Amino-1-carboxypentyl)iminodiacetic acid, AB-NTA) to produce pyrene-nitrilotriacetic acid (pyrene-NTA). The attached NTA group is able to chelate with metal ions such as Cu^{2+} or Ni^{2+} , which then can then coordinate with polyhistidine-tags attached to a protein [75]–[77]. Use of Cu^{2+} ions over Ni^{2+} gives stronger histidine bonding and less non-specific adsorption [77]. Functionalisation using the NTA- Ni^{2+} chemistry was successfully used to attach mammalian odorant receptors to a single carbon nanotube for detection of eugenol vapour in real-time [11]. Pyrene-biotin (pyrene butanol biotin ester) can also be produced for attaching avidin or streptavidin [75]. As avidin and streptavidin are tetrameric, they can be attached to both pyrene-biotin and biotinylated avi-tagged proteins simultaneously via strong non-covalent bonding, therefore linking the

1. Verifying Non-Covalent Functionalisation of Carbon Nanotubes and Graphene

transducer and receptor [78]–[81]. As the presence of his-tags and avi-tags on proteins can be readily controlled, these methods offer improved specificity and directionality over the traditional amide bonding seen earlier.

It is also possible to attach polyethylene glycol (PEG) chains to a pyrene group and modify them with reactive groups such as NTA and biotin to attach proteins in the manner outlined in the previous paragraph [82], [83]. Once modified with PEG, the water solubility of pyrene linkers increases, making it possible to perform a full functionalisation procedure exclusively in aqueous solution [82]. By setting the length of the PEG chain, the size of the linker molecule can be controlled - selection of a short chain is important for ensuring attached receptors remain within the Debye length of the transducer [3]. Functionalisation of a graphene transducer with pyrene-PEG-biotin has previously been used to bind streptavidin to a graphene field-effect transistor device [84]. The PEGylated linkers used in the following sections were purchased pre-prepared. Pyrene-PEG-NTA (2 kDa) was purchased from Nanocs, while pyrene-PEG-FITC (2 kDa, 10 kDa), pyrene-PEG-rhodamine (3.4 kDa), mPEG-Pyrene (10 kDa) and pyrene-PEG-biotin (10 kDa) were purchased from Creative PEGworks.

1.5.2. Fluorescence Characterisation with Pyrene-PEG-FITC

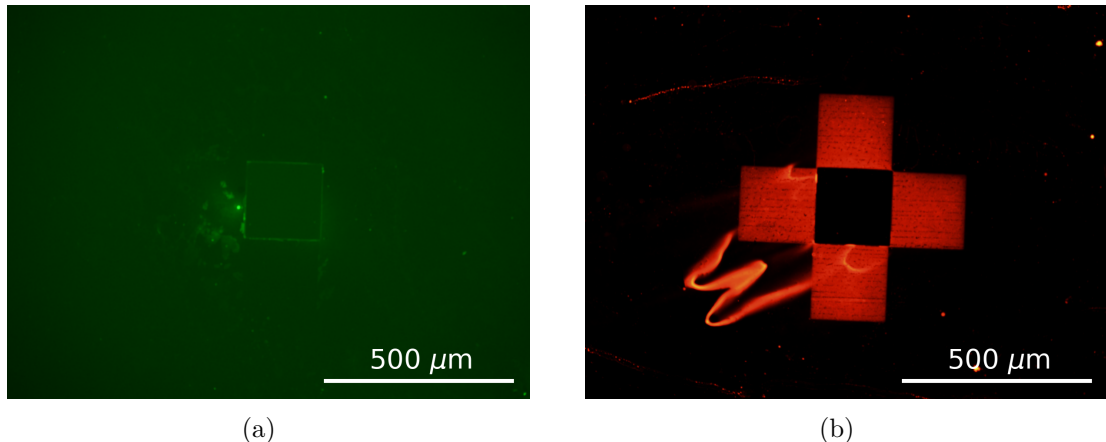


Figure 1.7.: Four $200 \mu\text{m} \times 200 \mu\text{m}$ graphene squares modified with the dyes (a) fluorescein isothiocyanate (FITC) and (b) Rhodamine B. No pyrene/PEG/pyrene-PEG was attached to these dyes. In (a), an FITC filter and 6.5 s exposure time was used, and in (b) a Texas Red filter and 1.4 s exposure time was used.

Dye attachment was used to map the presence of PEGylated pyrene-based linkers across a carbon nanotube or graphene surface with fluorescence microscopy. Four $200 \mu\text{m} \times 200 \mu\text{m}$ graphene squares were incubated in two commonly used and easily obtained

1.5. Attachment of PEGlyated Pyrene-Based Linkers

dyes, fluorescein isothiocyanate (FITC) and Rhodamine B, to test whether the dyes themselves bond to graphene.

The functionalisation of graphene devices with fluorescent dye was performed using the following steps:

1. 1 mM dye (FITC or Rhodamine B) prepared in PBS solution by vortex mixing for 10-15 minutes.
2. Graphene on silicon dioxide substrate rinsed with acetone and IPA, then nitrogen dried, and then treated with 300 mTorr 5W oxygen plasma for 15 s (see Section 1.6.2).
3. Immediately (in less than 1 min) place a 20 μ L droplet of dye solution onto the substrate surface, near wet tecwipes to keep droplets humidified, covered with a glass container. Leave for 20 minutes.
4. After 20 minutes, substrate rinsed in PBS for 30 s.
5. Substrate rinsed with m-CNT dispersion solution for 5 minutes at 70°C with a pipette, then rinsed with DI water, ethanol, acetone, IPA and nitrogen dried (see Section 1.6.3).

The results of this test are shown in Figure 1.7. There is a much stronger contrast between the graphene squares and the background after functionalisation with Rhodamine B, showing a clear, specific interaction between Rhodamine B and graphene. It has previously been determined that the benzene rings of rhodamine π -stack with carbon rings [85]. Rhodamine B could therefore not be used as a fluorescent marker to check for attachment of our linker molecules. However, as fluorescein isothiocyanate did not show significant interaction with the graphene, this marker was subsequently used for fluorescent mapping linker attachment. Figure 1.8 shows various concentrations of pyrene-PEG-FITC dissolved in 1XPBS, which is used for fluorescence characterisation in this section.

Both SU8 and AZ® 1518 photoresist were found to fluoresce, which is due to their photoactive component [86]. This passive fluorescence was found to drown out fluorescence from a dye-functionalised device channel, and so photoresist encapsulated devices were not used for fluorescence imaging. A different type of encapsulation could potentially be used to verify linker attachment with fluorescence after a device has been encapsulated. These alternative encapsulation methods for use with fluorescence microscopy are discussed in **?@sec-future-work**.

The functionalisation of graphene devices with pyrene-PEG-FITC was performed as follows:

1. 1 mM pyrene-PEG-FITC was prepared in ethanol by sonication for 1 minute then vortex mixing for 10-15 minutes, to fully dissolve the pyrene-PEG-FITC (Note:

1. Verifying Non-Covalent Functionalisation of Carbon Nanotubes and Graphene

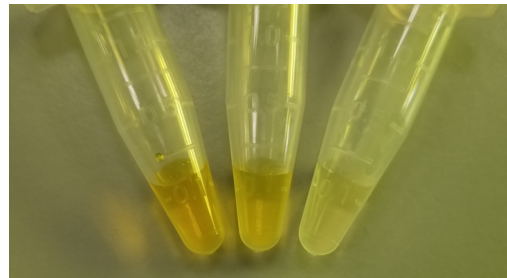


Figure 1.8.: Microcentrifuge tubes containing various concentrations of 10 kDa pyrene-PEG-FITC in solution (1 mM, 0.1 mM and 0.01 mM left to right)

pyrene-PEG-FITC is stored frozen, should be defrosted under vacuum 15 minutes before use).

2. Unencapsulated device was rinsed with acetone and IPA, then nitrogen dried.
3. The device was then fully submerged in pyrene-PEG-FITC/ethanol solution for 20 minutes.
4. After 20 minutes, device was rinsed for 30 s with ethanol, then acetone, IPA and nitrogen dried.

Fluorescence images of the unencapsulated graphene devices successfully functionalised with pyrene-PEG-FITC (PPF), showing up bright green against a dark background, are shown in Figure 1.9. As indicated by the labels, the darkest regions are the titanium-gold electrodes, and the bright green region is the PPF functionalised graphene channel. It is noticeable that some variation in fluorescence is seen between channels, indicating the quality of functionalisation may vary across the channels of a device. Some of the difficulties encountered when investigating functionalisation with pyrene-PEG-FITC are discussed later in Section 1.6.

<!—>

1.5.3. Electrical Characterisation with mPEG-Pyrene

?@fig-pypeg-dirac-shift compares the electrical characteristics of graphene transistor channels before and after functionalisation with various concentrations of mPEG-pyrene, showing the magnitude in shift of the (major) Dirac point. 2 mM Pyrene-PEG was dissolved in 1XPBS using a vortex mixer for 10 min at 1000 rpm until fully dissolved, then diluted in series to 1 mM, 0.1 mM, and 0.01 mM in 1XPBS. Plasma treated devices were treated with 5 W oxygen plasma for 15 s at 350 mTorr before functionalisation. 2 μ L solution was placed on each device channel for 1 hour, covered with a glass dish and in the presence of wet tecwipes to keep the environment humid. Devices were then rinsed in 1XPBS for 30 s before measurements were taken. Surfactant rinsing involved placing

1.5. Attachment of PEGylated Pyrene-Based Linkers

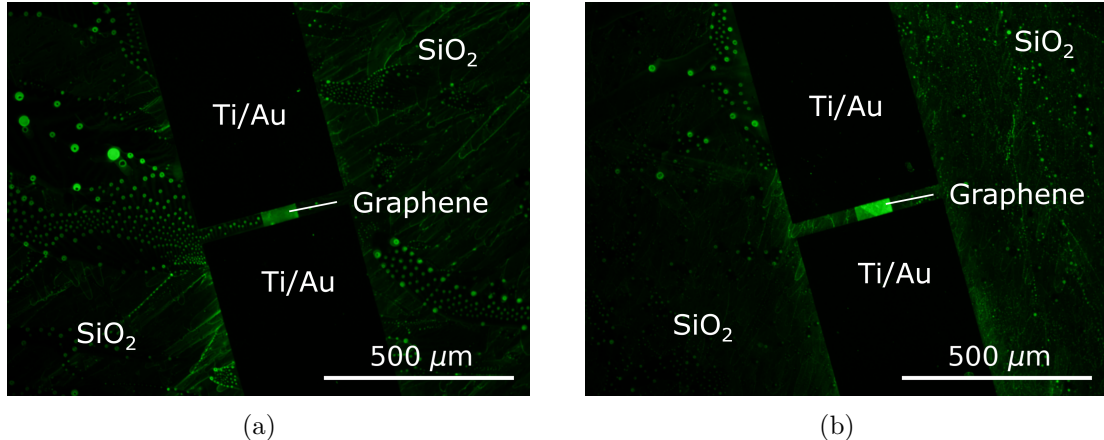


Figure 1.9.: Fluorescence images of an unencapsulated graphene channel after functionalisation with 1 mM pyrene-PEG-FITC in ethanol, taken using an FITC filter with a 1 s exposure time, where (a) shows channel 2 of the device and (b) shows channel 7. The darker regions are the device electrodes, while the brightly fluorescent region is the graphene channel area.

functionalised devices in m-CNT dispersion solution for 5 minutes at 70°C, periodically agitating the solution with a pipette, then rinsing the devices with DI water, ethanol, acetone, IPA and finally nitrogen drying them.

As in the case of PBASE and PBA on carbon nanotubes, the neutral charge of pyrene means there is no significant Dirac shift when the plasma treated devices are successfully functionalised with mPEG-pyrene [74]. Interestingly, however, when the devices are not plasma treated before functionalisation, there is a significant Dirac shift at higher concentrations of mPEG-pyrene. Since aqueous functionalisation without a plasma pre-treatment results in little or no graphene surface coverage, as demonstrated in Section 1.5.2, it can be safely assumed that this shift is due to attachment of mPEG-pyrene to the small region of silicon dioxide not covered by encapsulation which borders the channel. Furthermore, Section 1.5.2 shows us that even after plasma treatment, the SiO₂ surface will still interact with mPEG-pyrene upon functionalisation. Oxygen plasma treatment is known to make the graphene layer permeable to water, and therefore it is likely the SiO₂ surface below the graphene is also coated with mPEG-pyrene after plasma treatment [87]. Therefore, it appears the Dirac shift results from a difference in mPEG-pyrene surface coverage when comparing the SiO₂ surface next to the graphene channel and the SiO₂ below the graphene channel. The physical mechanism linking these two factors is currently unclear.

<!—>

1. Verifying Non-Covalent Functionalisation of Carbon Nanotubes and Graphene

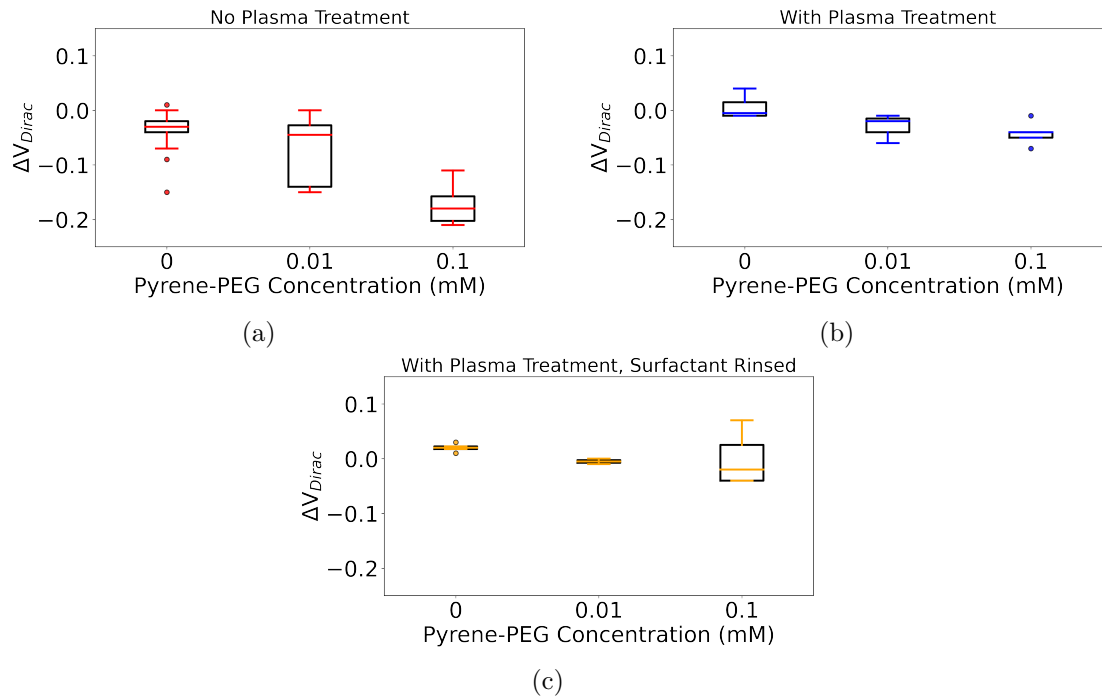


Figure 1.10.: (Major) Dirac voltage shifts of graphene field-effect transistors after functionalisation with concentrations of mPEG-Pyrene in 1XPBS at 0, 0.01 and 0.1 mM, followed by rinsing with m-surfactant solution. Measurements corresponding to each concentration are of three different device channels from a single device measured four times, where the device was rinsed with 1XPBS between each measurement.

1.6. Addressing Functionalisation Issues

1.6.1. Photoresist Contamination

An functionalisation issue quickly encountered when characterising pyrene-PEG-FITC interaction with device channels (PPF) via fluorescence microscopy was an unwanted secondary interaction between the linker and residual photoresist. Figure 1.11a and Figure 1.11b are fluorescence images of SU8 encapsulation before and after being exposed to PPF. Despite the same microscope settings being used to take the images (filter, ISO, contrast, exposure time), the SU8 exposed to PPF appears much brighter than the pristine SU8. No fluorescence is seen from the device channel, as the length of exposure time required to see the fluorescence would lead to fluorescence from the dye-modified linker attached to the photoresist flooding the image with light. An analogy which could be used is that of a dim outdoor lamp in a photograph; if the photograph was taken on a starless night, it would show up clearly, but with the sun out it would be very difficult to see regardless of how the photograph was taken. We therefore assert that because the fluorescence of the dye attached to the photoresist is much more intense than the dye attached to the carbon nanotubes, the linker appears to have a more extensive interaction with the photoresist via an unknown mechanism than it does by *pi*-stacking with the carbon nanotubes.

In Figure 1.11c that patches of photoresist residue remaining on a carbon nanotube film shows up brightly under the fluorescence microscope after being exposed to PPF. The presence of photoresist residue is undesirable for both functionalisation and sensing, and fluorescence microscopy was a useful tool for detecting residue and testing suitable residue elimination measures.

A similar interaction between AZ® 1518 photoresist and fluorescent-tagged, amine-terminated aptamer was seen when functionalising using PBASE. Two carbon nanotube network devices were spincoated with AZ® 1518 photoresist and heated at 95°C for 5 minutes. One device was then hardbaked at 200°C for 1 hour. Both devices were then rinsed for 1 minute with acetone. Each device was then submerged in 1 mM PBASE in methanol for 1 hour, rinsed with methanol and Tris buffer, then incubated in 1 µM Cy3-tagged aptamer in Tris buffer at 4°C overnight. The aptamer was denatured by heating in a water bath at 95°C for 5 minutes then cooling in an ice bath for 10 minutes before use. Fluorescence microscope images of channels from the two devices are shown in [?@fig-aptamer-photoresist](#), where the dark regions are the gold device electrodes.

From comparing Figure 1.11d and Figure 1.11e, it is apparent that hardbaking the AZ® 1518 photoresist significantly reduces the amount of fluorescent aptamer attached to the surface. This is an indication that the chemical interaction between the photoresist and the pyrene linker, or alternatively the biological material, can be suppressed through sufficient heating of the photoresist. Hardbaking of the photoresist does not appear to have completely prevented functionalisation, with some aptamer fluorescence still visible in Figure 1.11e. It is possible that heating from the bottom of the device is insufficient to

1. Verifying Non-Covalent Functionalisation of Carbon Nanotubes and Graphene

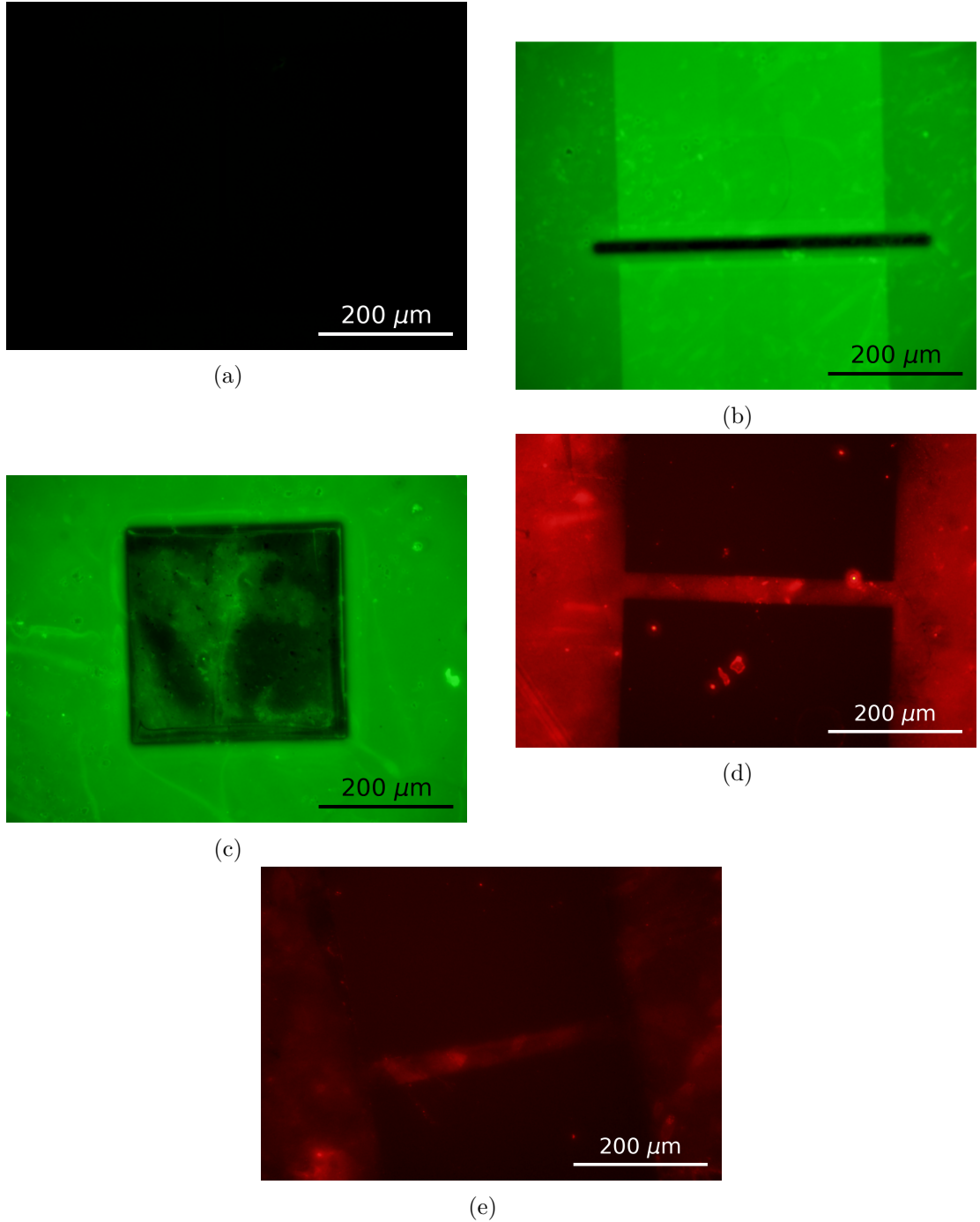


Figure 1.11.: A fluorescence image of a carbon nanotube device encapsulated with SU8 using the pre-2023 mask is shown in (a) using a 0.35 s exposure time. With the same exposure time as in (a), (c) shows a SU8-encapsulated channel after modification with an aqueous solution of 1 mM Pyrene-PEG-FITC, while (d) shows an SU8-coated CNT film where a $320 \mu\text{m} \times 320 \mu\text{m}$ region of SU8 has been photolithographically removed to expose the CNTs in that region. Both (d) and (e) show fluorescence images of an carbon nanotube device with photoresist surface residue after exposure to PBASE and fluorescent-tagged aptamer, where the device in (e) was hardbaked at 200°C for 1 hour before exposure while the device (d) was not. For images (a)-(c) a FITC filter was used, while for (d)-(e) a mCherry filter and 30 s exposure time were used.

1.6. Addressing Functionalisation Issues

hardbake the photoresist layer completely, an effect that would be amplified for the thick photoresist layer on encapsulated devices. Therefore, from June 2023 onwards devices were vacuum annealed for 1 hour at 150 °C prior to functionalisation. This approach was taken to ensure photoresist was being heated from above as well as below and made chemically inert at its surface.

Using fluorescence microscopy, an effective measure for remove exposed to UV light and placed in AZ® 326 developer to remove residual photoresist after each photolithography step.

1.6.2. Hydrophobicity of Carbon Nanotubes and Graphene

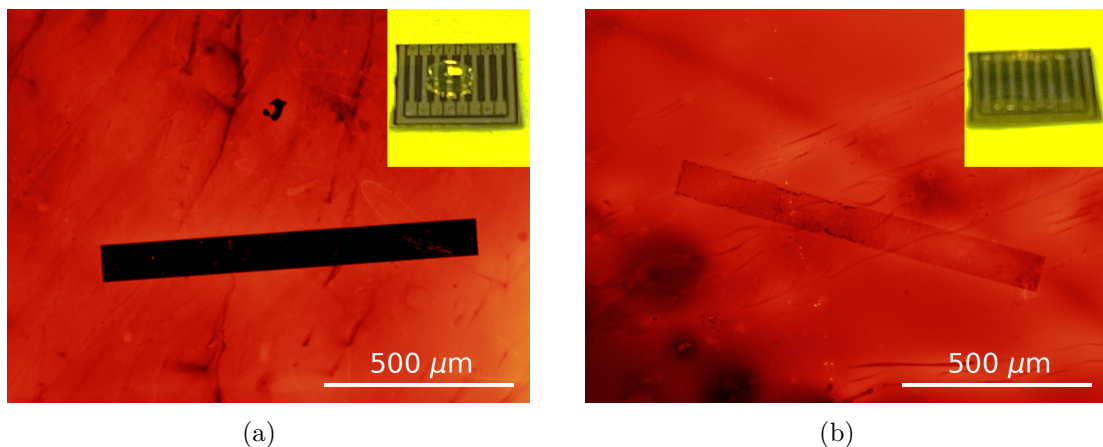


Figure 1.12.: Fluorescence images of a $1000 \mu\text{m} \times 100 \mu\text{m}$ graphene channel after functionalisation with 1 mM pyrene-PEG-rhodamine in 1XPBS, taken using a Texas Red filter and a 1.8 s exposure time. The graphene film in (a) was not oxygen plasma cleaned before functionalisation, while the graphene film in (b) was oxygen plasma cleaned at 5 W for 15 s at 300 mTorr pressure immediately before functionalisation. Insets show a 10 μL droplet placed on an unencapsulated carbon nanotube device before (a) and after (b) the same oxygen plasma treatment procedure.

As PEGylated linker dissolves well in aqueous solution, initial fluorescence imaging focused on functionalising devices with these linkers dissolved in 1XPBS. It was hoped that by keeping the device channels in a pH-controlled environment, the channel surface would be made more suitable for the attached receptors. Figure 1.12a shows a graphene film after exposure to pyrene-PEG-rhodamine (PPR) in 1XPBS solution for 1 hour. The pyrene-PEG-rhodamine has interacted with the silicon dioxide substrate (discussed further in Section 1.6.3) but not the graphene film. The graphene does not attach to the pyrene or rhodamine due to the highly hydrophobic graphene surface repelling the surrounding solution, preventing π -stacking from occurring. The hydrophobicity of the

1. Verifying Non-Covalent Functionalisation of Carbon Nanotubes and Graphene

graphene surface is not intrinsic to graphene (or to carbon nanotubes), and instead results from a hydrocarbonaceous layer which forms on the graphene (or carbon nanotube) surface when exposed to air [88]–[90]. Treatment with oxygen plasma at 5 W for 15 s has previously been found to remove this hydrocarbonaceous layer, restoring the intrinsic hydrophilicity of graphene [91]. Storing the graphene surface in DI water rather than air prevents the return of this hydrocarbon layer [88]. The use of a relatively low power plasma ensures damage to the graphene layer is minimised.

Treatment of an unencapsulated carbon nanotube network device at 5 W for 15 s at 300 mTorr greatly reduced the contact angle of a water droplet placed on the device surface, shown inset in Figure 1.12 before and after plasma treatment. A graphene film was then functionalised with pyrene-PEG-rhodamine in 1XPBS in the same manner as for the film in Figure 1.12a, except with the same plasma treatment performed on the film less than 1 minute before functionalisation. The result is shown in Figure 1.12b. The graphene now appears to interact with the pyrene-PEG-rhodamine. These results both indicate that the plasma treatment is increasing the hydrophilicity of the device surface, improving the ability of pyrene-PEG-rhodamine to π -stack with graphene. The disadvantage of this procedure is that the plasma cleaning introduces defects to the graphene surface which may be undesirable for device electrical behaviour. Furthermore, it was often found that devices functionalised in this manner had their conductance drop significantly after functionalisation, even though plasma treatment itself did not significantly alter device conductance. Solvent was therefore used for the initial linker functionalisation in Section 1.7, as it did not require a plasma cleaning step for successful attachment.

1.6.3. Substrate Interaction with Linker Molecules

Another issue that arose when verifying surface functionalisation was the interaction between pyrene linker and the silicon dioxide substrate. This interaction meant it was difficult to discern whether the pyrene group was interacting in a specific manner with the channel film. It was confirmed that pyrene-PEG was interacting with silicon dioxide, rather than residual photoresist or nanomaterial, by performing a pyrene-PEG-rhodamine functionalisation on pristine silicon dioxide, as shown in Figure 1.13b. The PEGlyated linker supplier suggested that the surface should be thoroughly rinsed with surfactant to remove weakly-bound pyrene-PEG-FITC attached to the silicon dioxide, while preserving the pyrene-PEG-FITC strongly attached via π -stacking to the graphene or carbon nanotube film [92]. The following process was then used to remove pyrene-PEG-FITC from the silicon dioxide: the film was rinsed with DI water for 30 s, then placed in m-CNT dispersion solution (NanoIntegris) for 5 minutes at 70°C while agitating with a pipette, and finally rinsed with DI water, ethanol, acetone, IPA and nitrogen dried. The results of this thorough cleaning process are shown in Figure 1.13c and Figure 1.13d. The majority of pyrene-PEG-FITC was removed in regions with no graphene, but remained where graphene was present, indicating specific, π -stacking interaction took place between the pyrene-PEG-FITC and graphene.

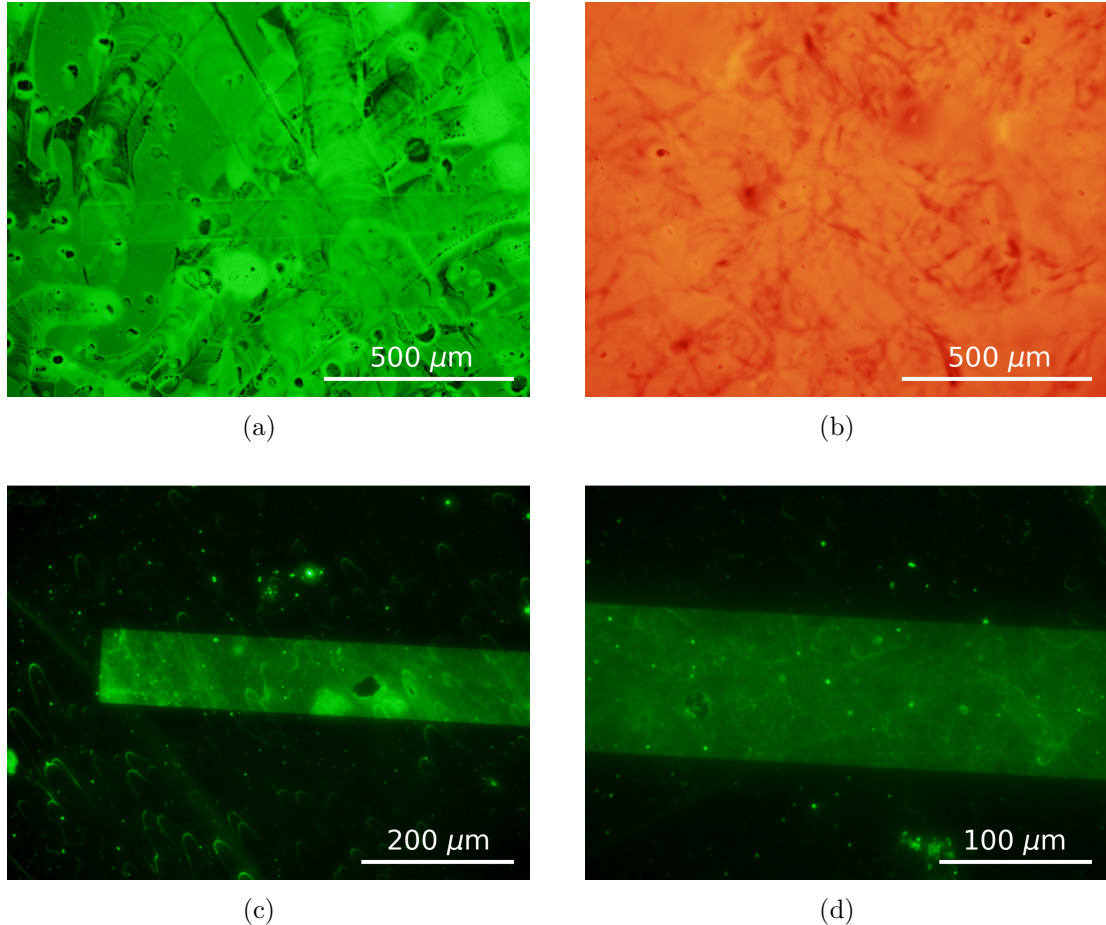


Figure 1.13.: The $1000 \mu\text{m} \times 100 \mu\text{m}$ graphene film in image (a) was functionalised with 1 mM pyrene-PEG-FITC in 1XPBS after oxygen plasma treatment, taken using an FITC filter and a 1.6 s exposure time. (b) shows a silicon dioxide surface which had never been exposed to carbon nanotubes, graphene or photoresist after exposure to 1 mM pyrene-PEG-rhodamine in 1XPBS, taken using a Texas Red filter and a 1.8 s exposure time. Graphene films on a substrate functionalised with 1 mM pyrene-PEG-FITC in 1XPBS after oxygen plasma treatment then cleaned with m-CNT dispersion surfactant (NanoIntegris) are shown in (c) and (d), where a FITC filter was used, with 7.5 s and 7.75 s exposure times respectively.

1. Verifying Non-Covalent Functionalisation of Carbon Nanotubes and Graphene

1.6.4. “Coffee-Ring” Effect

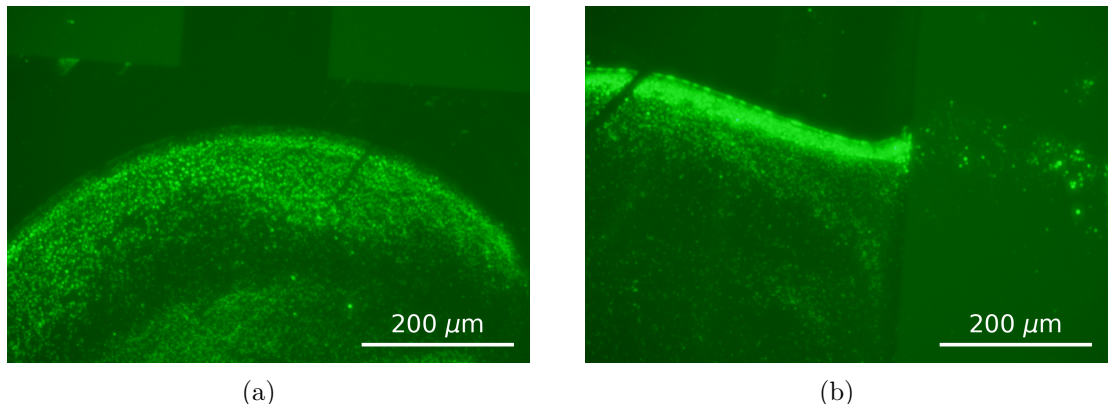


Figure 1.14.: Both (a) and (b) show a build-up of his-tag GFP at the edges of the droplet region where pyrene-PEG-NTA had been present, taken using an GFP filter and a 5 s exposure time. On the right hand side of (b), no his-tag GFP is visible on the metal electrode, as no pyrene-PEG attaches to the metal electrodes.

From Table 1.1, full device submersion appears to be the most common approach for functionalisation with solution containing linker molecules like PBASE. However, some groups placed small droplets of solution onto the device channels when functionalisation, and this approach was tested as part of the fluorescence verification work. For functionalisation with his-tagged green fluorescent protein, after plasma cleaning at 5 W for 15 s at 300 mTorr, a 4 μ L droplet of 100 μ M pyrene-PEG-NTA in 1XPBS was placed on each graphene device channel and left covered in a humid environment for 15 minutes. The device was then rinsed with 1XPBS, submerged in 10 mM NiSO₄ in 1XPBS for 1 hour, rinsed in 1XPBS then submerged in 10 mL of 100 ng/mL his-tag GFP solution (Thermofisher) overnight. Fluorescence microscope imaging showed that a ring of biomaterial would build up around the outer edge of regions where pyrene-PEG-NTA had been present, as seen in Figure 1.14.

It appears this is a result of the his-tag GFP attaching to a dense region of pyrene-PEG-NTA at the edge of the functionalisation droplet. This accretion of pyrene-PEG-NTA at the edge of the droplet is a result of the coffee-ring effect, where the evaporation of the droplet leads to transport of particles to the droplet edges via capillary flow [93], [94]. As the effects of having a large gradient in the surface coverage of attached protein across the device surface have unknown consequences for sensing, in functionalisation processes performed after this test the devices were incubated with PBASE or pyrene-PEG-NTA by submerging them in solution, rather than using the dropcasting approach.

1.7. Verifying Linker-OR Nanodisc Attachment

1.7.1. Functionalisation using PBASE

To verify the formation of amide (or imide) bonds between PBASE and the odorant receptors (ORs) contained within nanodiscs, a fluorescent biomarker was directly attached to the odorant receptors for detection with fluorescence microscopy. The biomarker used was the *Aequorea Victoria* green fluorescent protein (GFP). As far as I know, this is the first time fluorescence has been used to verify the successful attachment of odorant receptor nanodiscs to a carbon nanotube network.

The functionalisation of unencapsulated carbon nanotube devices (steam-deposited, fabricated after June 2023) with PBASE and GFP-OR Nanodiscs was performed as follows:

1. The device was exposed to UV light for 1 minute, placed in AZ® 326 developer for 3 minutes, then rinsed with acetone, isopropanol and nitrogen dried.
2. The device was vacuum annealed for 1 hour at 150°C (Note: Steps 1 & 2 were added to ensure any residual photoresist on the channel was removed or passivated before functionalisation, see Section 1.6.1).
3. A solution of 1 mM PBASE (Setareh Biotech) in methanol prepared by fully dissolving 2 mg PBASE in 5 mL methanol by vortex mixing at 1000 rpm in a dark room (Note: PBASE was stored at -18°C for 18 months prior to use, and was thawed under vacuum for 15 minutes in dark conditions before opening)
4. The device was then rinsed with methanol, fully submerged in ~ 1 mL of PBASE in methanol solution and left covered with parafilm for 1 hour, then rinsed with methanol for 15 s, rinsed with 1XPBS for 15 s and nitrogen dried to remove residual PBASE.
5. The device was left dry and in darkness while collecting the GFP-OR nanodiscs from the -80°C freezer.
6. 20 μ L GFP-OR nanodiscs (batch number ND-GFP-OR43b-0002, prepared 12 months earlier) was diluted in 2 mL 1XPBS (Note: The full 2 mL was used to flush out the nanodisc vial when preparing the nanodisc solution, with successive additions and subtractions of 50 μ L 1XPBS into and from the vial).
7. The device was submerged in the GFP-OR43b nanodisc solution and left covered with parafilm for 1 hour, then rinsed with 1XPBS for 15 s.
8. For fluorescence microscopy, the device was briefly rinsed with DI water and nitrogen dried to remove salt residue from the 1XPBS.

1. Verifying Non-Covalent Functionalisation of Carbon Nanotubes and Graphene

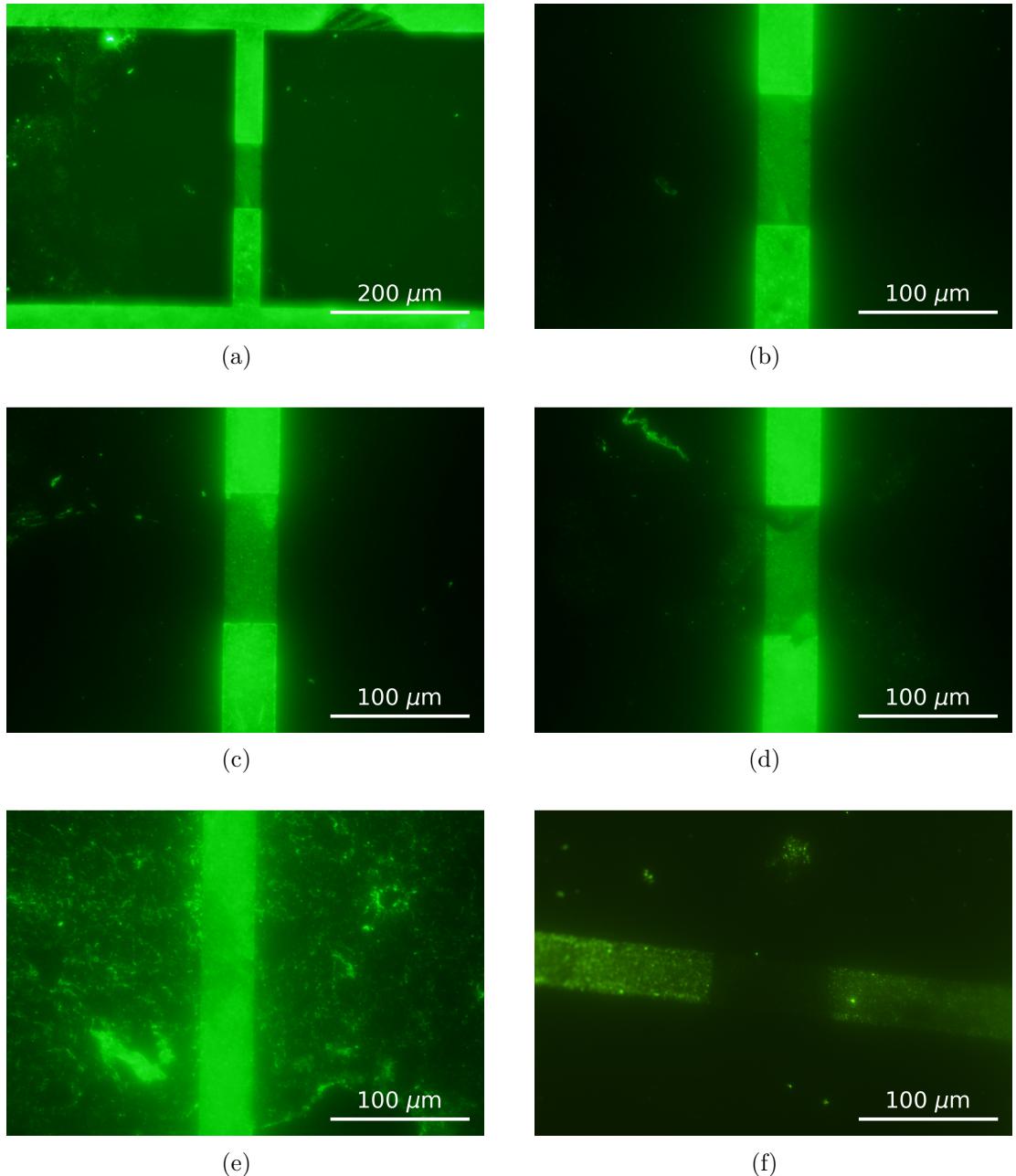


Figure 1.15.: Fluorescence images of an unencapsulated carbon nanotube network channel after functionalisation with 1 mM PBASE in methanol, followed by 10 μ L/mL GFP-OR43b nanodiscs in 1XPBS.(a) and (b) show channel 1 of the device, (c) shows channel 2, (d) shows channel 3 and (e) shows channel 6. The image in (f) was taken of a separate device functionalised using 0.1 mM PBASE. All images were taken using an GFP filter and a 10 s exposure time.

1.7. Verifying Linker-OR Nanodisc Attachment

Fluorescence images of the unencapsulated carbon nanotube devices successfully functionalised with GFP-OR43b nanodiscs using PBASE are shown in Figure 1.15a-e.

As in Section 1.5.2, dark regions are the gold electrodes. There clearly appears to be an attachment between the GFP-OR43b nanodiscs and the silicon dioxide surface. As this device has been annealed, UV exposed and developed before functionalisation, this non-specific attachment is unlikely to be interaction with residual photoresist (see Section 1.6.1). Instead it appears that the pyrene, nanodiscs or both are directly interacting with the silicon dioxide surface. Fluorescence in the channel region in Figure 1.15a-e indicates GFP-OR43b nanodiscs are present on or around the carbon nanotubes. The fluorescence brightness was consistent across four out of eight channels on the 1 mM PBASE functionalised device. The other four channels looked similar to Figure 1.15e, where nanodiscs appeared to be present in excess on both the channel, SiO_2 , and even on the gold electrodes. This is an indication that the concentration of GFP-OR43b used should be lowered further for a more consistent functionalisation.

Figure 1.15f shows that a lowered concentration of PBASE leads to a channel region with no visible fluorescence (with a 10 s exposure time). This indicates that the PBASE solution used to incubate the device must be sufficiently concentrated for odorant receptors to interact with the channel region. As discussed in Section 1.6.3, this indicates that a specific interaction is occurring between PBASE and the GFP-OR43b.

1.7.2. Functionalisation using Pyrene-PEG-NTA

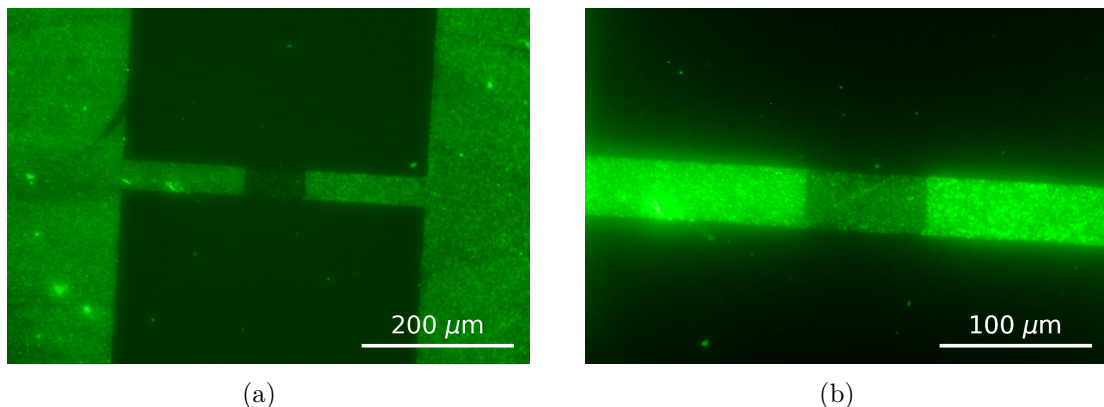


Figure 1.16.: Image (a) and (b) show fluorescence images of a carbon nanotube channel after functionalisation with 1 $\mu\text{L}/\text{mL}$ GFP-OR43b nanodiscs in 1XPBS using pyrene-PEG-NTA. (b) has been brightened by 40% for visual clarity. Both images were taken using a GFP filter and 10 s exposure time.

Pyrene-PEG-NTA was also used to attach the green fluorescent protein tagged odorant receptors through attaching to their histidine tag via the mechanisms outlined in Section 1.5.1. As nanodiscs as well as odorant receptors have attached amine groups

1. Verifying Non-Covalent Functionalisation of Carbon Nanotubes and Graphene

(see ?@sec-artificial-membranes), even nanodiscs which do not contain the receptor required for sensing can attach to the carbon nanotubes in the presence of PBASE linker. However, the nanodiscs used here possessed no histidine tag. Therefore, successful GFP-OR Nanodisc attachment via a histidine bonding process indicates odorant receptors, rather than nanodisc membranes, have specifically attached to the carbon nanotube network.

The following procedure was used to functionalise unencapsulated carbon nanotube devices (steam-deposited, fabricated after June 2023) with pyrene-PEG-NTA and GFP-OR nanodiscs:

1. The device was exposed to UV light for 1 minute, placed in AZ® 326 developer for 3 minutes, then rinsed with acetone, isopropanol and nitrogen dried.
2. The device was vacuum annealed for 1 hour at 150°C (Note: Steps 1 & 2 were added to ensure any residual photoresist on the channel was removed or passivated before functionalisation, see Section 1.6.1).
3. A solution of 100 μ M Pyrene-PEG-NTA (Nanocs) in ethanol was prepared by fully dissolving 1 mg Pyrene-PEG-NTA in 5 mL ethanol by sonicating for 1 minute in a dark room (Note: Pyrene-PEG-NTA was stored at -18°C for 6 months prior to use, and was thawed under vacuum for 15 minutes in dark conditions before opening; the solution was left at 4°C for a week before use).
4. 10 mL of 10 mM CuSO₄ in 1XPBS was prepared by dissolving CuSO₄ powder in 1XPBS by vortex mixing for 15 minutes.
5. After vortex mixing Pyrene-PEG-NTA in ethanol solution at 1000 rpm for 10 minutes, the Pyrene-PEG-NTA solution was diluted to 1 μ M in ethanol by placing 100 μ L into 9.9 mL ethanol.
6. The device was then rinsed with acetone, IPA and nitrogen dried, fully submerged in 10 mL of 1 μ M Pyrene-PEG-NTA in ethanol solution and left covered with parafilm for 15 minutes, then rinsed with ethanol for 15 s, rinsed with 1XPBS for 15 s and nitrogen dried to remove residual Pyrene-PEG-NTA.
7. The device was then placed in 10 mL of CuSO₄ in 1XPBS and covered with parafilm for 1 hour to coordinate Cu²⁺ with NTA, then rinsed 15 with 1XPBS (Note: NiSO₄ can be used as an alternative)
8. 10 μ L GFP-OR nanodiscs were diluted in 10 mL 1XPBS (batch number ND-GFP-OR43b-0002, prepared 12 months earlier and stored at -80°C) .
9. The device was submerged in the GFP-OR43b nanodisc solution and left covered with parafilm for 30 minutes, then rinsed with 1XPBS for 15 s.
10. For fluorescence microscopy, the device was rinsed with DI water for 1 minute and nitrogen dried to remove salt residue from the 1XPBS.

Fluorescence images of the unencapsulated carbon nanotube devices successfully functionalised with GFP-OR43b nanodiscs using Pyrene-PEG-NTA are shown in Figure 1.16a-b. Similar non-specific attachment to the silicon dioxide as in Section 1.7.1 is seen, but there is clear attachment of green fluorescent protein-modified odorant receptors in the channel. Device characteristics were measured with a multimeter to check how the device characteristics changed during the functionalisation process. The minimum measured channel resistance increased from $560\text{ k}\Omega$ to $790\text{ k}\Omega$, indicating the functionalisation process tends to decrease channel conductance.

1.8. Conclusions

It has been well-established in the literature that the π -stacking reaction mechanism between pyrene-based linkers and graphene and carbon nanotube network field-effect transistors can be used to create working biosensors. The previous use of various linker molecules for biosensor functionalisation was investigated. Despite the wide use of 1-pyrenebutanoic acid N-hydroxysuccinimide ester (PBASE) and 1-pyrenebutyric acid (PBA) for functionalisation of biosensors, the literature shows a significant variation in the methods used for attachment of linker molecules to a transistor channel. The most common methods, using 6 mM PBASE dissolved in dimethylformamide or 1 mM PBASE in methanol, stem directly from the first documented use of PBASE for functionalisation of carbon nanotube biosensors. In the last 6 years, more research has been done into optimising the PBASE methodology for graphene devices, but there is still disagreement in the literature over whether minimising or maximising PBASE coverage on a graphene device channel is desirable for sensing. Due to disagreement in the literature around suitable non-covalent methods for biosensor functionalisation, several steps were taken to identify a rapid and simple method for verifying successful functionalisation, and to locate any potential barriers to a successful functionalisation.

I first compared the advantages and disadvantages of the various linker molecules under investigation. The use of hydrogen NMR gave indications that water was present in PBASE samples prepared in DMSO. Concerns around the impact of the hydrolysis of PBASE on functionalisation mean that the presence of water is strongly undesirable. An alternative functionalisation approach less prone to hydrolysis is the reaction of PBA with EDC in the presence of NHS. However, this process has its own disadvantages, such as undesirable protein interactions and the increased amount of steps and process variables involved. Pyrene-NTA is also less prone to hydrolysis than PBASE but unlike PBASE or PBA/EDC interacts with a specific protein tag, the histidine tag. PEGylation of the pyrene-NTA linker also means that the entire functionalisation process can be performed in aqueous solution, avoiding the introduction of non-organic solvents. This approach is desirable, since the non-aqueous solvents traditionally used for functionalisation may have negative impacts on device behaviour. For example, carbon nanotube device channel transfer characteristics were found to undergo a significant shift of $\Delta V = -0.15 \pm 0.02$ when exposed to DMSO or MeOH for 1 hour.

1. Verifying Non-Covalent Functionalisation of Carbon Nanotubes and Graphene

Next, I verified that the pyrene groups of the linker molecules of interest were attaching successfully to either carbon nanotubes or graphene. Raman spectroscopy showed that incubating a highly-bundled carbon nanotube film in 5 mM PBASE or PBA in DMSO for 1 hour increased I_D/I_G by a factor of ~ 3 relative to the DMSO-only case. Incubating a steam-deposited carbon nanotube device in a 1 mM concentration of PBASE in methanol or DMSO for 1 hour was found to cause a significant increase in device on-current relative to the solvent-only case, and a similar increase in on-current was seen for 5 mM PBA in DMSO relative to the DMSO-only case. When a PBA-functionalised device was placed in aqueous solution with 20 mM EDC and 40 mM NHS for 30 minutes, a further increase in on-current was seen. Fluorescence microscopy was used to demonstrate the successful attachment of pyrene-PEG to graphene using an attached FITC probe, where immersing a graphene film in 1 mM pyrene-PEG in ethanol led to the channels becoming brightly fluorescent relative to the background using a 1 s exposure time. Pyrene-PEG was found to have little impact on the Dirac voltage of successfully functionalised graphene devices.

Finally, I verified that the linkers were successfully attaching the odorant receptors to the device channels with fluorescence microscopy. Various obstacles to successful functionalisation were encountered and addressed. Photoresist contamination was addressed with exposure and development steps before functionalisation (no exposure for SU8 encapsulated devices). Hydrophobicity of graphene films was addressed by plasma treatment before functionalisation in aqueous solution. A surfactant rinse was used to distinguish between weak substrate-linker interaction and π -stacking between linker and the channel. Finally, coffee-ring distribution of linker was addressed by always submerging the device in linker when functionalising. Once these issues were addressed, two processes were identified which could be demonstrated to be successful using fluorescence microscopy. The first used an initial submersion in 1 mM PBASE in methanol for 1 hour, then submersion in $10 \mu\text{L mL}^{-1}$ OR43b nanodiscs in 1XPBS for 1 hour. The second used a submersion in $1 \mu\text{L}$ pyrene-PEG-NTA in ethanol for 15 minutes, then submersion in 10 mM CuSO₄ in 1XPBS for 1 hour, then submersion in $1 \mu\text{L mL}^{-1}$ OR43b nanodiscs in 1XPBS for 30 minutes.

A. Python Code for Data Analysis

A.1. Code Repository

The code used for general analysis of field-effect transistor devices in this thesis was written with Python 3.8.8. Contributors to the code used include Erica Cassie, Erica Happe, Marissa Dierkes and Leo Browning. The code is located on GitHub and the research group OneDrive, and is available on request.

A.2. Atomic Force Microscope Histogram Analysis

The purpose of this code is to analyse atomic force microscope (AFM) images of carbon nanotube networks in .xyz format taken using an atomic force microscope and processed in Gwyddion (see [?@sec-afm-characterisation](#)). It was originally designed by Erica Happe in Matlab, and adapted by Marissa Dierkes and myself for use in Python. The code imports the .xyz data and sorts it into bins 0.15 nm in size for processing. To perform skew-normal distribution fits, both *scipy.optimize.curve_fit* and *scipy.stats.skewnorm* modules are used in this code.

A.3. Raman Spectroscopy Analysis

The purpose of this code is to analyse a series of Raman spectra taken at different points on a single film (see [?@sec-raman-characterisation](#)). Data is imported in a series of tab-delimited text files, with the low wavenumber spectrum ($100\text{ cm}^{-1} - 650\text{ cm}^{-1}$) and high wavenumber spectrum ($1300\text{ cm}^{-1} - 1650\text{ cm}^{-1}$) imported in separate datafiles for each scan location.

A.4. Field-Effect Transistor Analysis

The purpose of this code is to analyse electrical measurements taken of field-effect transistor (FET) devices. Electrical measurements were either taken from the Keysight 4156C Semiconductor Parameter Analyser, National Instruments NI-PXIe or Keysight B1500A Semiconductor Device Analyser as discussed in [?@sec-electrical-characterisation](#);

A. Python Code for Data Analysis

the code is able to analyse data taken from all three measurement setups. The main Python file in the code base consists of three related but independent modules: the first analyses and plots sensing data from the FET devices, the second analyses and plots transfer characteristics from channels across a device, and the third compares individual channel characteristics before and after a modification or after each of several modifications. The code base also features a separate config file and style sheet which govern the behaviour of the main code. The code base was designed collaboratively by myself and Erica Cassie over GitHub using the Sourcetree Git GUI.

The first of the three modules is for processing sensing datasets. This module imports sensing measurements in .csv format and analyses them, then outputs a plot of the raw data, alongside multiple plots which have been modified in various ways. It can also fit exponential and linear trendlines to regions of the sensing data, as well as find the signal change per analyte addition, and returns spreadsheets containing the results of these analyses. These spreadsheets include the standard deviation for all included parameters. Modified plots include normalised plots (type of normalisation can be set in config file), plots with fitted curves, plots with the linear baseline drift removed, plots of signal with analyte addition, “despiked” plots and “filtered” plots. It is possible to add annotations to any of these plots using the config file, and it is possible to produce a plot with a combination of these modifications.

The `scipy.optimize.curve_fit` module is used to fit linear and exponential curves to regions of interest of the sensing data. Initial parameters for the `scipy.optimize.curve_fit` module are chosen by approximating fitting parameters in a similar manner to the approach in Section A.2. For a linear fit $mt + b$, the parameters are simply set as $m = 1$ and $b = 0$. For an exponential fit $a \exp(-t/\tau) + c$, c is set as the final current measurement of the region of interest and a is set as the initial current measurement minus c . Then, τ is set as the time where current has dropped to $e^{-1}a + c$.

“Despiked” plots have had spurious datapoints removed through the use of an interquartile range rolling filter. The window size of the rolling filter used was 40 datapoints, and datapoints in each window with a z-score above ± 3 were removed from the plotted/processed data. “Filtered” plots had noise reduced using a moving median filter. The moving median filter is more effective at removing noise than a simple moving average, and has advantages over other filters (such as the Savitzky-Golay filter) when removing noise from data with sharp edges, as is the case for sensing data. Median filtering can also be used for baseline drift compensation, though this approach was not used in this thesis [95]. The moving median filter used had a window of 40 datapoints.

Plots of signal with analyte addition were constructed from current data after first removing baseline drift and applying a moving median filter. A simple difference calculation between the mean of the filtered current before an addition and the mean of the filtered current after the addition was performed at each addition. These differences were then normalised relative to the initial current. The signal with analyte addition give reasonably consistent results regardless of whether baseline drift was removed from the data,

A.4. Field-Effect Transistor Analysis

as shown in Figure A.1. We can therefore be confident that robust signal with analyte addition plots are robust even in the presence of significant drift.

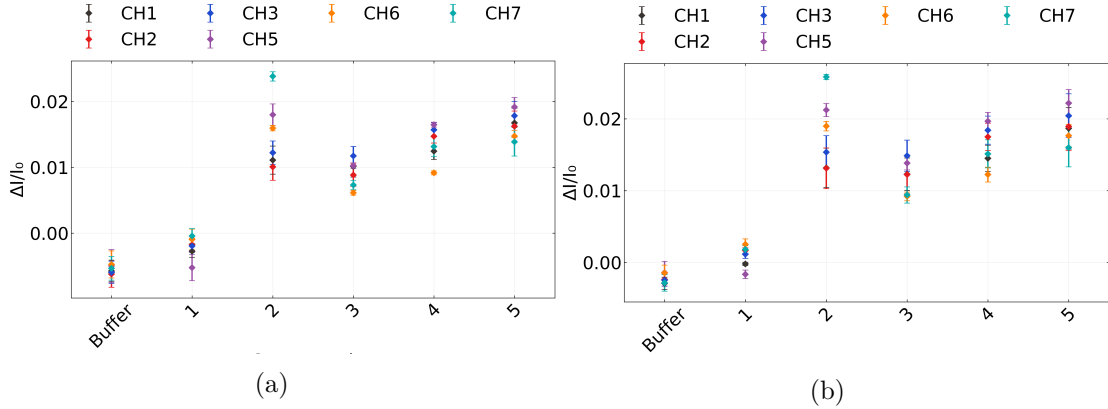


Figure A.1.: A comparison of signal with analyte addition plots taken from the same salt concentration sensing dataset (the same dataset as used in [?@fig-salt-conc-sensing](#)). In (a), a simple difference calculation performed on filtered data was used, while in (b) the same calculation was performed on filtered data with the baseline drift removed, the method used in the body of the thesis.

The second module imports transfer measurements in .csv format and creates combined and individual plots of the eight channels on a single device. In combined plots, channels which are non-working, due to being shorted or non-conducting, are removed via setting a maximum and minimum possible on-current in the config file. Various parameters from the transfer characteristics are saved as a spreadsheet along with standard error. These parameters include on current, off current, subthreshold slope and threshold voltage for the carbon nanotube devices, and on current, off current and major Dirac point voltage for graphene devices. The device type being analysed can be set in the config file.

The third module imports several transfer measurements in .csv format and allows for comparison of the same channel before and after some modification. It also calculates the shift in either threshold voltage or major Dirac voltage of the device.

Bibliography

- [1] Niazul I. Khan and Edward Song. "Detection of an IL-6 Biomarker Using a GFET Platform Developed with a Facile Organic Solvent-Free Aptamer Immobilization Approach". In: *Sensors 2021*, Vol. 21, Page 1335 21.4 (Feb. 2021), p. 1335. ISSN: 1424-8220. DOI: 10.3390/S21041335. URL: <https://www.mdpi.com/1424-8220/21/4/1335>.
- [2] Hong Phan T. Nguyen, Thanihaichelvan Murugathas, and Natalie O.V. Plank. "Comparison of Duplex and Quadruplex Folding Structure Adenosine Aptamers for Carbon Nanotube Field Effect Transistor Aptasensors". In: *Nanomaterials (Basel, Switzerland)* 11.9 (Sept. 2021). ISSN: 2079-4991. DOI: 10.3390/NANO11092280. URL: <https://pubmed.ncbi.nlm.nih.gov/34578596/>.
- [3] Bajramshahe Shkodra, Mattia Petrelli, Martina Aurora Costa Angeli, et al. "Electrolyte-gated carbon nanotube field-effect transistor-based biosensors: Principles and applications". In: *Applied Physics Reviews* 8.4 (Dec. 2021), p. 41325. ISSN: 19319401. DOI: 10.1063 / 5 . 0058591 / 1076095. URL: [/aip/apr/article/8/4/041325/1076095/Electrolyte-gated-carbon-nanotube-field-effect](https://aip/apr/article/8/4/041325/1076095/Electrolyte-gated-carbon-nanotube-field-effect).
- [4] Nikita Nekrasov, Natalya Yakunina, Averyan V. Pushkarev, et al. "Spectral-phase interferometry detection of ochratoxin a via aptamer-functionalized graphene coated glass". In: *Nanomaterials* 11.1 (Jan. 2021), pp. 1–10. ISSN: 20794991. DOI: 10.3390/nano11010226. URL: <https://www.mdpi.com/2079-4991/11/1/226>.
- [5] Vladyslav Mishyn, Adrien Hugo, Teresa Rodrigues, et al. "The holy grail of pyrene-based surface ligands on the sensitivity of graphene-based field effect transistors". In: *Sensors and Diagnostics* 1.2 (Mar. 2022), pp. 235–244. ISSN: 2635-0998. DOI: 10.1039/D1SD00036E. URL: <https://pubs.rsc.org/en/content/articlehtml/2022/sd/d1sd00036e>.
- [6] Erica Cassie, Hamish Dunham, Erica Happe, et al. "A comparison between oestradiol aptamers as receptors in CNT FET biosensors". In: *Sensors and Diagnostics* 2.6 (Nov. 2023), pp. 1561–1573. ISSN: 2635-0998. DOI: 10.1039/D3SD00055A. URL: [https://pubs.rsc.org/en/content/articlelanding/2023/sd/d3sd00055a](https://pubs.rsc.org/en/content/articlehtml/2023/sd/d3sd00055a).

Bibliography

- [7] Mitchell B. Lerner, Felipe Matsunaga, Gang Hee Han, et al. “Scalable production of highly sensitive nanosensors based on graphene functionalized with a designed G protein-coupled receptor”. In: *Nano Letters* 14.5 (May 2014), pp. 2709–2714. ISSN: 15306992. DOI: 10.1021/NL5006349/SUPPL_FILE/NL5006349_SI_001.PDF. URL: <https://pubs.acs.org/doi/full/10.1021/nl5006349>.
- [8] Sae Ryun Ahn, Ji Hyun An, Seung Hwan Lee, et al. “Peptide hormone sensors using human hormone receptor-carrying nanovesicles and graphene FETs”. In: *Scientific reports* 10.1 (Dec. 2020). ISSN: 2045-2322. DOI: 10.1038/S41598-019-57339-1. URL: <https://pubmed.ncbi.nlm.nih.gov/31942024/>.
- [9] Jing Tong, Lei Zhang, Yi Wang, et al. “High response photodetection by applying the optimized photoreceptor protein modification on graphene based field effect transistors”. In: *FrMat* 7 (July 2020), p. 222. ISSN: 22968016. DOI: 10.3389/FMATS.2020.00222. URL: <https://ui.adsabs.harvard.edu/abs/2020FrMat...7.222T/abstract>.
- [10] Shiyu Wang, Md Zakir Hossain, Kazuo Shinozuka, et al. “Graphene field-effect transistor biosensor for detection of biotin with ultrahigh sensitivity and specificity”. In: *Biosensors and Bioelectronics* 165 (Oct. 2020), p. 112363. ISSN: 18734235. DOI: 10.1016/J.BIOS.2020.112363. URL: [/pmc/articles/PMC7272179/](https://pmc/articles/PMC7272179/)?report=abstract%20https://www.ncbi.nlm.nih.gov/pmc/articles/PMC7272179/.
- [11] Brett R. Goldsmith, Joseph J. Mitala, Jesusa Josue, et al. “Biomimetic chemical sensors using nanoelectronic readout of olfactory receptor proteins”. In: *ACS Nano* 5.7 (July 2011), pp. 5408–5416. ISSN: 19360851. DOI: 10.1021/NN200489J/SUPPL_FILE/NN200489J_SI_001.PDF. URL: <https://pubs.acs.org/doi/full/10.1021/nn200489j>.
- [12] Minju Lee, Heehong Yang, Daesan Kim, et al. “Human-like smelling of a rose scent using an olfactory receptor nanodisc-based bioelectronic nose”. In: *Scientific reports* 8.1 (Dec. 2018). ISSN: 2045-2322. DOI: 10.1038/S41598-018-32155-1. URL: <https://pubmed.ncbi.nlm.nih.gov/30224633/>.
- [13] Thanihaichelvan Murugathas, Han Yue Zheng, Damon Colbert, et al. “Biosensing with Insect Odorant Receptor Nanodiscs and Carbon Nanotube Field-Effect Transistors”. In: *ACS Applied Materials and Interfaces* 11.9 (Mar. 2019), pp. 9530–9538. ISSN: 19448252. DOI: 10.1021/ACSAMI.8B19433. URL: <https://pubs.acs.org/doi/full/10.1021/acsami.8b19433>.
- [14] Thanihaichelvan Murugathas, Cyril Hamiaux, Damon Colbert, et al. “Evaluating insect odorant receptor display formats for biosensing using graphene field effect transistors”. In: *ACS Applied Electronic Materials* 2.11 (Nov. 2020), pp. 3610–3617. ISSN: 26376113. DOI: 10.1021/ACSAELM.0C00677/ASSET/IMAGES/LARGE/EL0C00677_0006.jpeg. URL: <https://pubs.acs.org/doi/full/10.1021/acsaelm.0c00677>.

- [15] Dongseok Moon, Yeon Kyung Cha, So ong Kim, et al. “FET-based nanobiosensors for the detection of smell and taste”. In: *Science China. Life sciences* 63.8 (Aug. 2020), pp. 1159–1167. ISSN: 1869-1889. DOI: 10.1007/S11427-019-1571-8. URL: <https://pubmed.ncbi.nlm.nih.gov/31974862/>.
- [16] Jin Yoo, Daesan Kim, Heehong Yang, et al. “Olfactory receptor-based CNT-FET sensor for the detection of DMMP as a simulant of sarin”. In: *Sensors and Actuators B: Chemical* 354 (Mar. 2022), p. 131188. ISSN: 0925-4005. DOI: 10.1016/J.SNB.2021.131188.
- [17] Brenda Long, Mary Manning, Micheal Burke, et al. “Non-Covalent Functionalization of Graphene Using Self-Assembly of Alkane-Amines”. In: *Advanced Functional Materials* 22.4 (Feb. 2012), pp. 717–725. ISSN: 1616-3028. DOI: 10.1002/ADFM.201101956. URL: <https://onlinelibrary.wiley.com/doi/full/10.1002/adfm.201101956> % 20<https://onlinelibrary.wiley.com/doi/abs/10.1002/adfm.201101956>.
- [18] Antonello Di Crescenzo, Valeria Ettorre, and Antonella Fontana. “Non-covalent and reversible functionalization of carbon nanotubes”. In: *Beilstein Journal of Nanotechnology* 5.1 (2014), p. 1675. ISSN: 21904286. DOI: 10.3762/BJNANO.5.178. URL: [/pmc/articles/PMC4222398/](https://pmc/articles/PMC4222398/) % 20<https://www.ncbi.nlm.nih.gov/pmc/articles/PMC4222398/>.
- [19] Kishan Thodkar, Pierre Andre Cazade, Frank Bergmann, et al. “Self-assembled pyrene stacks and peptide monolayers tune the electronic properties of functionalized electrolyte-gated graphene field-effect transistors”. In: *ACS Applied Materials and Interfaces* 13.7 (Feb. 2021), pp. 9134–9142. ISSN: 19448252. DOI: 10.1021/ACSAU.0C18485/ASSET/IMAGES/LARGE/AM0C18485_0006.JPG. URL: <https://pubs.acs.org/doi/full/10.1021/acsami.0c18485>.
- [20] Carbonnanotube. *File:Noncovalent carboncarbonnanotube.png*. 2015. URL: https://en.m.wikipedia.org/wiki/File:Noncovalent_carboncarbonnanotube.png (visited on 2023-10-13).
- [21] Emilio M. Pérez and Nazario Martín. “ $\pi-\pi$ interactions in carbon nanostructures”. In: *Chemical Society Reviews* 44.18 (Sept. 2015), pp. 6425–6433. ISSN: 1460-4744. DOI: 10.1039/C5CS00578G. URL: <https://pubs.rsc.org/en/content/articlehtml/2015/cs/c5cs00578g> % 20<https://pubs.rsc.org/en/content/articlelanding/2015/cs/c5cs00578g>.
- [22] Chelsea R. Martinez and Brent L. Iverson. “Rethinking the term “pi-stacking””. In: *Chemical Science* 3.7 (June 2012), pp. 2191–2201. ISSN: 2041-6539. DOI: 10.1039/C2SC20045G. URL: <https://pubs.rsc.org/en/content/articlehtml/2012/sc/c2sc20045g> % 20<https://pubs.rsc.org/en/content/articlelanding/2012/sc/c2sc20045g>.
- [23] Greg T. Hermanson. “Buckyballs, Fullerenes, and Carbon Nanotubes”. In: *Bioconjugate Techniques* (Jan. 2013), pp. 741–755. DOI: 10.1016/B978-0-12-382239-0.00016-9.

Bibliography

- [24] Yan Zhou, Yi Fang, and Ramaraja P. Ramasamy. “Non-Covalent Functionalization of Carbon Nanotubes for Electrochemical Biosensor Development”. In: *Sensors (Basel, Switzerland)* 19.2 (Jan. 2019). ISSN: 1424-8220. DOI: 10.3390/S19020392. URL: <https://pubmed.ncbi.nlm.nih.gov/30669367/>.
- [25] J. A. M. J. Frisch and G. W. Trucks and H. B. Schlegel and G. E. Scuseria and M. A. Robb and J. R. Cheeseman and G. Scalmani and V. Barone and G. A. Petersson and H. Nakatsuji and X. Li and M. Caricato and A. V. Marenich and J. Bloino and B. G. Janesko and R. G, J. E. Peralta, F. Ogliaro, et al. *Gaussian^16 Revision C.01.* 2016.
- [26] Yasuhiro Oishi, Hirotugu Ogi, Satoshi Hagiwara, et al. “Theoretical Analysis on the Stability of 1-Pyrenebutanoic Acid Succinimidyl Ester Adsorbed on Graphene”. In: *ACS Omega* 7.35 (Sept. 2022), pp. 31120–31125. ISSN: 24701343. DOI: 10.1021/AC SOMEWA.2C03257 / ASSET / IMAGES / LARGE / AO2C03257_0004. JPEG. URL: <https://pubs.acs.org/doi/full/10.1021/acsomewa.2c03257>.
- [27] Kenzo Maehashi, Taiji Katsura, Kagan Kerman, et al. “Label-free protein biosensor based on aptamer-modified carbon nanotube field-effect transistors”. In: *Analytical Chemistry* 79.2 (Jan. 2007), pp. 782–787. ISSN: 00032700. DOI: 10.1021/ac060830g. URL: <https://pubs.acs.org/doi/full/10.1021/ac060830g>.
- [28] Cristina García-Aljaro, Lakshmi N. Cella, Dhamanand J. Shirale, et al. “Carbon nanotubes-based chemiresistive biosensors for detection of microorganisms”. In: *Biosensors and Bioelectronics* 26.4 (Dec. 2010), pp. 1437–1441. ISSN: 09565663. DOI: 10.1016/j.bios.2010.07.077.
- [29] R. J. Chen, Y. Zhang, D. Wang, et al. “Noncovalent sidewall functionalization of single-walled carbon nanotubes for protein immobilization”. In: *Journal of the American Chemical Society* 123.16 (2001), pp. 3838–3839. ISSN: 00027863. DOI: 10.1021/ja010172b. URL: <http://pubs.acs.org..>
- [30] Lakshmi N. Cella, Pablo Sanchez, Wenwan Zhong, et al. “Nano aptasensor for Protective Antigen Toxin of Anthrax”. In: *Analytical Chemistry* 82.5 (Mar. 2010), pp. 2042–2047. ISSN: 00032700. DOI: 10.1021/ac902791q. URL: <https://pubs.acs.org/doi/full/10.1021/ac902791q>.
- [31] Basanta K. Das, Chaker Tlili, Sushmee Badhulika, et al. “Single-walled carbon nanotubes chemiresistor aptasensors for small molecules: Picomolar level detection of adenosine triphosphate”. In: *Chemical Communications* 47.13 (Mar. 2011), pp. 3793–3795. ISSN: 1364548X. DOI: 10.1039/c0cc04733c. URL: <https://pubs.rsc.org/en/content/articlehtml/2011/cc/c0cc04733c%20https://pubs.rsc.org/en/content/articlelanding/2011/cc/c0cc04733c>.
- [32] Koen Besteman, Jeong O. Lee, Frank G.M. Wiertz, et al. “Enzyme-coated carbon nanotubes as single-molecule biosensors”. In: *Nano Letters* 3.6 (June 2003), pp. 727–730. ISSN: 15306984. DOI: 10.1021/NL034139U. URL: <https://pubs.acs.org/doi/full/10.1021/nl034139u>.

- [33] Deana Kwong Hong Tsang, Tyler J. Lieberthal, Clare Watts, et al. “Chemically Functionalised Graphene FET Biosensor for the Label-free Sensing of Exosomes”. In: *Scientific Reports* 9.1 (Sept. 2019), pp. 1–10. ISSN: 20452322. DOI: 10.1038/s41598-019-50412-9. URL: <https://www.nature.com/articles/s41598-019-50412-9>.
- [34] Gregory R. Wiedman, Yanan Zhao, Arkady Mustaev, et al. “An Aptamer-Based Biosensor for the Azole Class of Antifungal Drugs”. In: *mSphere* 2.4 (Aug. 2017). ISSN: 23795042. DOI: 10.1128/msphere.00274-17. URL: /pmc/articles/PMC5566834 / %20 / pmc / articles / PMC5566834 / ?report = abstract % 20https : //www.ncbi.nlm.nih.gov/pmc/articles/PMC5566834/.
- [35] Zhaoli Gao, Han Xia, Jonathan Zauberman, et al. “Detection of Sub-fM DNA with Target Recycling and Self-Assembly Amplification on Graphene Field-Effect Biosensors”. In: *Nano Letters* 18.6 (June 2018), pp. 3509–3515. ISSN: 15306992. DOI: 10.1021/acs.nanolett.8b00572. URL: <https://pubs.acs.org/doi/full/10.1021/acs.nanolett.8b00572>.
- [36] Michael T. Hwang, B. Landon Preston, Lee Joon, et al. “Highly specific SNP detection using 2D graphene electronics and DNA strand displacement”. In: *Proceedings of the National Academy of Sciences of the United States of America* 113.26 (June 2016), pp. 7088–7093. ISSN: 10916490. DOI: 10.1073/pnas.1603753113. URL: <https://www.pnas.org/doi/abs/10.1073/pnas.1603753113>.
- [37] Zhuang Hao, Yunlu Pan, Cong Huang, et al. “Modulating the Linker Immobilization Density on Aptameric Graphene Field Effect Transistors Using an Electric Field”. In: *ACS Sensors* 5.8 (Aug. 2020), pp. 2503–2513. ISSN: 23793694. DOI: 10.1021/ACSENSORS.0C00752/ASSET/IMAGES/LARGE/SE0C00752_0008. JPEG. URL: <https://pubs.acs.org/doi/full/10.1021/acssensors.0c00752>.
- [38] Mohd Maidin Nur Nasyifa, A. Rahim Ruslinda, Nur Hamidah Abdul Halim, et al. “Immuno-probed graphene nanoplatelets on electrolyte-gated field-effect transistor for stable cortisol quantification in serum”. In: *Journal of the Taiwan Institute of Chemical Engineers* 117 (Dec. 2020), pp. 10–18. ISSN: 18761070. DOI: 10.1016/j.jtice.2020.12.008.
- [39] Rui Campos, Jérôme Borme, Joana Rafaela Guerreiro, et al. “Attomolar label-free detection of dna hybridization with electrolyte-gated graphene field-effect transistors”. In: *ACS Sensors* 4.2 (Feb. 2019), pp. 286–293. ISSN: 23793694. DOI: 10.1021/acssensors.8b00344. URL: <https://pubs.acs.org/doi/full/10.1021/acssensors.8b00344>.
- [40] Murat Kuscu, Hamideh Ramezani, Ergin Dinc, et al. “Graphene-based Nanoscale Molecular Communication Receiver: Fabrication and Microfluidic Analysis”. In: (June 2020). arXiv: 2006.15470. URL: <https://arxiv.org/abs/2006.15470v2>.
- [41] Shicai Xu, Jian Zhan, Baoyuan Man, et al. “Real-time reliable determination of binding kinetics of DNA hybridization using a multi-channel graphene biosensor”. In: *Nature Communications* 8.1 (Mar. 2017), pp. 1–10. ISSN: 20411723. DOI: 10.1038/ncomms14902. URL: <https://www.nature.com/articles/ncomms14902>.

Bibliography

- [42] Niazul I. Khan, Mohammad Mousazadehkasin, Sujoy Ghosh, et al. “An integrated microfluidic platform for selective and real-time detection of thrombin biomarkers using a graphene FET”. In: *Analyst* 145.13 (June 2020), pp. 4494–4503. ISSN: 13645528. DOI: 10.1039/d0an00251h. URL: <https://pubs.rsc.org/en/content/articlehtml/2020/an/d0an00251h%20https://pubs.rsc.org/en/content/articlelanding/2020/an/d0an00251h>.
- [43] T Ono, K Kamada, R Hayashi, et al. “Lab-on-a-graphene-FET detection of key molecular events underpinning influenza 2 virus infection and effect of antiviral drugs 3 Running title: Graphene-FET detects reactions in an influenza infection MAIN TEXT”. In: *bioRxiv* (Mar. 2020), p. 2020.03.18.996884. DOI: 10.1101/2020.03.18.996884. URL: <https://doi.org/10.1101/2020.03.18.996884>.
- [44] Han Yue Zheng, Omar A. Alsager, Bicheng Zhu, et al. “Electrostatic gating in carbon nanotube aptasensors”. In: *Nanoscale* 8.28 (July 2016), pp. 13659–13668. ISSN: 20403372. DOI: 10.1039/c5nr08117c. URL: <https://pubs.rsc.org/en/content/articlehtml/2016/nr/c5nr08117c%20https://pubs.rsc.org/en/content/articlelanding/2016/nr/c5nr08117c>.
- [45] Jun Pyo Kim, Byung Yang Lee, Joohyung Lee, et al. “Enhancement of sensitivity and specificity by surface modification of carbon nanotubes in diagnosis of prostate cancer based on carbon nanotube field effect transistors”. In: *Biosensors and Bioelectronics* 24.11 (July 2009), pp. 3372–3378. ISSN: 09565663. DOI: 10.1016/j.bios.2009.04.048. URL: <https://pubmed.ncbi.nlm.nih.gov/19481922/>.
- [46] Jagriti Sethi, Michiel Van Bulck, Ahmed Suhail, et al. “A label-free biosensor based on graphene and reduced graphene oxide dual-layer for electrochemical determination of beta-amyloid biomarkers”. In: *Microchimica Acta* 187.5 (May 2020), pp. 1–10. ISSN: 14365073. DOI: 10.1007/s00604-020-04267-x. URL: <https://link.springer.com/article/10.1007/s00604-020-04267-x>.
- [47] Yasuhide Ohno, Kenzo Maehashi, and Kazuhiko Matsumoto. “Label-free biosensors based on aptamer-modified graphene field-effect transistors”. In: *Journal of the American Chemical Society* 132.51 (Dec. 2010), pp. 18012–18013. ISSN: 00027863. DOI: 10.1021/ja108127r. URL: <https://pubs.acs.org/doi/full/10.1021/ja108127r>.
- [48] Ryan J. Lopez, Sofia Babanova, Kateryna Artyushkova, et al. “Surface modifications for enhanced enzyme immobilization and improved electron transfer of PQQ-dependent glucose dehydrogenase anodes”. In: *Bioelectrochemistry* 105 (Oct. 2015), pp. 78–87. ISSN: 1878562X. DOI: 10.1016/j.bioelechem.2015.05.010. URL: <https://pubmed.ncbi.nlm.nih.gov/26011132/>.
- [49] Guinevere Strack, Robert Nichols, Plamen Atanassov, et al. “Modification of carbon nanotube electrodes with 1-pyrenebutanoic acid, succinimidyl ester for enhanced bioelectrocatalysis”. In: *Methods in Molecular Biology* 1051 (2013), pp. 217–228. ISSN: 10643745. DOI: 10.1007/978-1-62703-550-7_14. URL: <https://pubmed.ncbi.nlm.nih.gov/23934807/>.

- [50] Greg T. Hermanson. “The Reactions of Bioconjugation”. In: *Bioconjugate Techniques* (Jan. 2013), pp. 229–258. DOI: 10.1016/B978-0-12-382239-0.00003-0.
- [51] Malcolm Hinnemo, Jie Zhao, Patrik Ahlberg, et al. “On Monolayer Formation of Pyrenebutyric Acid on Graphene”. In: *Langmuir* 33.15 (Apr. 2017), pp. 3588–3593. ISSN: 15205827. DOI: 10.1021/ACS.LANGMUIR.6B04237/ASSET/IMAGES/LARGE/LA-2016-04237V_0003.JPG. URL: <https://pubs.acs.org/doi/full/10.1021/acs.langmuir.6b04237>.
- [52] Xue V. Zhen, Emily G. Swanson, Justin T. Nelson, et al. “Noncovalent monolayer modification of graphene using pyrene and cyclodextrin receptors for chemical sensing”. In: *ACS Applied Nano Materials* 1.6 (June 2018), pp. 2718–2726. ISSN: 25740970. DOI: 10.1021/acsanm.8b00420. URL: <https://pubs.acs.org/doi/full/10.1021/acsanm.8b00420>.
- [53] Ryan J. White, Noelle Phares, Arica A. Lubin, et al. “Optimization of electrochemical aptamer-based sensors via optimization of probe packing density and surface chemistry”. In: *Langmuir : the ACS journal of surfaces and colloids* 24.18 (Sept. 2008), pp. 10513–10518. ISSN: 0743-7463. DOI: 10.1021/LA800801V. URL: <https://pubmed.ncbi.nlm.nih.gov/18690727/>.
- [54] Yu Chen, Tze Sian Pui, Patthara Kongsuphol, et al. “Aptamer-based array electrodes for quantitative interferon- γ detection”. In: *Biosensors and Bioelectronics* 53 (Mar. 2014), pp. 257–262. ISSN: 1873-4235. DOI: 10.1016/J.BIOS.2013.09.046. URL: <https://pubmed.ncbi.nlm.nih.gov/24144556/>.
- [55] Greg T. Hermanson. “Homobifunctional Crosslinkers”. In: *Bioconjugate Techniques* (Jan. 2013), pp. 275–298. DOI: 10.1016/B978-0-12-382239-0.00005-4.
- [56] 1-Pyrenebutyric acid N-hydroxysuccinimide ester - [1H NMR] - Spectrum - SpectraBase. URL: <https://spectrabase.com/spectrum/FxRoJanrm9t> (visited on 2023-10-19).
- [57] R. G. Lebel and D. A.I. Goring. “Density, Viscosity, Refractive Index, and Hygroscopicity of Mixtures of Water and Dimethyl Sulfoxide”. In: *Journal of Chemical and Engineering Data* 7.1 (Jan. 1962), pp. 100–101. ISSN: 15205134. DOI: 10.1021/JE60012A032/ASSET/JE60012A032.FP.PNG_V03. URL: <https://pubs.acs.org/doi/abs/10.1021/je60012a032>.
- [58] Alexander B. Artyukhin, Michael Stadermann, Raymond W. Friddle, et al. “Controlled electrostatic gating of carbon nanotube FET devices”. In: *Nano Letters* 6.9 (Sept. 2006), pp. 2080–2085. ISSN: 15306984. DOI: 10.1021/NL061343J/SUPPLFILE/NL061343JSI20060609_104449.PDF. URL: <https://pubs.acs.org/doi/full/10.1021/nl061343j>.
- [59] Iddo Heller, Anne M. Janssens, Jaan Männik, et al. “Identifying the mechanism of biosensing with carbon nanotube transistors”. In: *Nano Letters* 8.2 (Feb. 2008), pp. 591–595. ISSN: 15306984. DOI: 10.1021/NL072996I/SUPPL_FILE/NL072996ISI20071116_124235.PDF. URL: <https://pubs.acs.org/doi/full/10.1021/nl072996i>.

Bibliography

- [60] M. Mohsen-Nia, H. Amiri, and B. Jazi. “Dielectric constants of water, methanol, ethanol, butanol and acetone: Measurement and computational study”. In: *Journal of Solution Chemistry* 39.5 (2010), pp. 701–708. ISSN: 00959782. DOI: 10.1007/S10953-010-9538-5.
- [61] Johannes Hunger, Richard Buchner, Mohamed E. Kandil, et al. “Relative permittivity of dimethylsulfoxide and N, N -dimethylformamide at temperatures from (278 to 328) K and pressures from (0.1 to 5) MPa”. In: *Journal of Chemical and Engineering Data* 55.5 (May 2010), pp. 2055–2065. ISSN: 00219568. DOI: 10.1021/JE9010773/SUPPL_FILE/JE9010773_SI_001.PDF. URL: <https://pubs.acs.org/doi/full/10.1021/je9010773>.
- [62] Ning Gao, Teng Gao, Xiao Yang, et al. “Specific detection of biomolecules in physiological solutions using graphene transistor biosensors”. In: *Proceedings of the National Academy of Sciences of the United States of America* 113.51 (Dec. 2016), pp. 14633–14638. ISSN: 10916490. DOI: 10.1073/PNAS.1625010114/SUPPL_FILE/PNAS.201625010SI.PDF. URL: <https://www.pnas.org/doi/abs/10.1073/pnas.1625010114>.
- [63] Kyoungseon Min, Jungbae Kim, Kyungmoon Park, et al. “Enzyme immobilization on carbon nanomaterials: Loading density investigation and zeta potential analysis”. In: *Journal of Molecular Catalysis B: Enzymatic* 83 (Nov. 2012), pp. 87–93. ISSN: 1381-1177. DOI: 10.1016/J.MOLCATB.2012.07.009.
- [64] Xuan Xu, Jiachao Yu, Jing Qian, et al. “Functionalization of nitrogen-doped carbon nanotubes by 1-pyrenebutyric acid and its application for biosensing”. In: *IEEE Sensors Journal* 14.7 (2014), pp. 2341–2346. ISSN: 1530437X. DOI: 10.1109/JSEN.2014.2309974.
- [65] Mercè Pacios, Iñigo Martin-Fernandez, Xavier Borrisé, et al. “Real time protein recognition in a liquid-gated carbon nanotube field-effect transistor modified with aptamers”. In: *Nanoscale* 4.19 (Sept. 2012), pp. 5917–5923. ISSN: 2040-3372. DOI: 10.1039/C2NR31257C. URL: <https://pubs.rsc.org/en/content/articlehtml/2012/nr/c2nr31257c%20https://pubs.rsc.org/en/content/articlelanding/2012/nr/c2nr31257c>.
- [66] Marcin S. Filipiak, Marcel Rother, Nesha M. Andoy, et al. “Highly sensitive, selective and label-free protein detection in physiological solutions using carbon nanotube transistors with nanobody receptors”. In: *Sensors and Actuators B: Chemical* 255 (Feb. 2018), pp. 1507–1516. ISSN: 0925-4005. DOI: 10.1016/J.SNB.2017.08.164.
- [67] Jie Liu, Florence Appaix, Olivier Bibari, et al. “Control of neuronal network organization by chemical surface functionalization of multi-walled carbon nanotube arrays”. In: *Nanotechnology* 22.19 (May 2011). ISSN: 1361-6528. DOI: 10.1088/0957-4484/22/19/195101. URL: <https://pubmed.ncbi.nlm.nih.gov/21436508/>.

- [68] Christoph Fenzl, Pranati Nayak, Thomas Hirsch, et al. “Laser-Scribed Graphene Electrodes for Aptamer-Based Biosensing”. In: *ACS sensors* 2.5 (May 2017), pp. 616–620. ISSN: 2379-3694. DOI: 10.1021 / ACSSENSORS.7B00066. URL: <https://pubmed.ncbi.nlm.nih.gov/28723173/>.
- [69] Deepak Sehgal and Inder K. Vijay. “A Method for the High Efficiency of Water-Soluble Carbodiimide-Mediated Amidation”. In: *Analytical Biochemistry* 218.1 (Apr. 1994), pp. 87–91. ISSN: 0003-2697. DOI: 10.1006/ABIO.1994.1144.
- [70] Greg T. Hermanson. “Zero-Length Crosslinkers”. In: *Bioconjugate Techniques* (Jan. 2013), pp. 259–273. DOI: 10.1016/B978-0-12-382239-0.00004-2.
- [71] Greg T. Hermanson. “Microparticles and Nanoparticles”. In: *Bioconjugate Techniques* (Jan. 2013), pp. 549–587. DOI: 10.1016/B978-0-12-382239-0.00014-5.
- [72] Gang Wei, Changjiang Pan, Jörg Reichert, et al. “Controlled assembly of protein-protected gold nanoparticles on noncovalent functionalized carbon nanotubes”. In: *Carbon* 48.3 (Mar. 2010), pp. 645–653. ISSN: 0008-6223. DOI: 10.1016 / J.CARBON.2009.10.006.
- [73] Meng Lan, Guoli Fan, Wei Sun, et al. “Synthesis of hybrid Zn–Al–In mixed metal oxides/carbon nanotubes composite and enhanced visible-light-induced photocatalytic performance”. In: *Applied Surface Science* 282 (Oct. 2013), pp. 937–946. ISSN: 0169-4332. DOI: 10.1016/J.APSUSC.2013.06.095.
- [74] Mitchell B. Lerner, James M. Resczenski, Akshay Amin, et al. “Toward quantifying the electrostatic transduction mechanism in carbon nanotube molecular sensors”. In: *Journal of the American Chemical Society* 134.35 (Sept. 2012), pp. 14318–14321. ISSN: 00027863. DOI: 10.1021/JA306363V/SUPPL_FILE/JA306363V_SI_001.PDF. URL: <https://pubs.acs.org/doi/full/10.1021/ja306363v>.
- [75] Michael Holzinger, Jessica Baur, Raoudha Haddad, et al. “Multiple functionalization of single-walled carbon nanotubes by dip coating”. In: *Chemical Communications* 47.8 (Feb. 2011), pp. 2450–2452. ISSN: 1364-548X. DOI: 10.1039/C0CC03928D. URL: <https://pubs.rsc.org/en/content/articlehtml/2011/cc/c0cc03928d%20https://pubs.rsc.org/en/content/articlelanding/2011/cc/c0cc03928d>.
- [76] Yoshihisa Amano, Ayako Koto, Shohei Matsuzaki, et al. “Construction of a biointerface on a carbon nanotube surface for efficient electron transfer”. In: *Materials Letters* 174 (July 2016), pp. 184–187. ISSN: 0167-577X. DOI: 10.1016/J.MATLET.2016.03.113.
- [77] Y. Y. Chang, H. Li, and H. Sun. “Immobilized Metal Affinity Chromatography (IMAC) for Metalloproteomics and Phosphoproteomics”. In: *Inorganic and Organometallic Transition Metal Complexes with Biological Molecules and Living Cells* (Jan. 2017), pp. 329–353. DOI: 10.1016/B978-0-12-803814-7.00009-5.

Bibliography

- [78] Alexander Star, Jean Christophe P. Gabriel, Keith Bradley, et al. “Electronic detection of specific protein binding using nanotube FET devices”. In: *Nano Letters* 3.4 (Apr. 2003), pp. 459–463. ISSN: 15306984. DOI: 10.1021/NL0340172/SUPPL_FILE/NL0340172SI20030213_114154.PDF. URL: <https://pubs.acs.org/doi/full/10.1021/nl0340172>.
- [79] Christopher M. Dundas, Daniel Demonte, and Sheldon Park. “Streptavidin-biotin technology: Improvements and innovations in chemical and biological applications”. In: *Applied Microbiology and Biotechnology* 97.21 (Nov. 2013), pp. 9343–9353. ISSN: 01757598. DOI: 10.1007/S00253-013-5232-Z/FIGURES/3. URL: <https://link.springer.com/article/10.1007/s00253-013-5232-z>.
- [80] Greg T. Hermanson. “(Strept)avidin–Biotin Systems”. In: *Bioconjugate Techniques* (Jan. 2013), pp. 465–505. DOI: 10.1016/B978-0-12-382239-0.00011-X.
- [81] Michael Fairhead and Mark Howarth. “Site-specific biotinylation of purified proteins using BirA”. In: *Methods in molecular biology (Clifton, N.J.)* 1266 (2015), p. 171. ISSN: 10643745. DOI: 10.1007/978-1-4939-2272-7_12. URL: /pmc/articles/PMC4304673/%20/pmc/articles/PMC4304673/?report=abstract%20https://www.ncbi.nlm.nih.gov/pmc/articles/PMC4304673/.
- [82] Greg T. Hermanson. “PEGylation and Synthetic Polymer Modification”. In: *Bioconjugate Techniques* (Jan. 2013), pp. 787–838. DOI: 10.1016/B978-0-12-382239-0.00018-2.
- [83] Mehdi Meran, Pelin Deniz Akkus, Ozge Kurkcuoglu, et al. “Noncovalent Pyrene-Polyethylene Glycol Coatings of Carbon Nanotubes Achieve in Vitro Biocompatibility”. In: *Langmuir* 34.40 (Oct. 2018), pp. 12071–12082. ISSN: 15205827. DOI: 10.1021/ACS.LANGMUIR.8B00971. URL: <https://pubs.acs.org/doi/full/10.1021/acs.langmuir.8b00971>.
- [84] Hiroko Miki, Atsunobu Isobayashi, Tatsuro Saito, et al. “Ionic liquids with wafer-scalable graphene sensors for biological detection”. In: *IEEE Transactions on Nanobioscience* 18.2 (Apr. 2019), pp. 216–219. ISSN: 15361241. DOI: 10.1109/TNB.2019.2905286.
- [85] Zhenghai Tang, Yanda Lei, Baochun Guo, et al. “The use of rhodamine B-decorated graphene as a reinforcement in polyvinyl alcohol composites”. In: *Polymer* 53.2 (Jan. 2012), pp. 673–680. ISSN: 0032-3861. DOI: 10.1016/J.POLYMER.2011.11.056.
- [86] Jeng Hao Pai, Yuli Wang, Gina To A. Salazar, et al. “A Photoresist with Low Fluorescence for Bioanalytical Applications”. In: *Analytical chemistry* 79.22 (Nov. 2007), p. 8774. ISSN: 00032700. DOI: 10.1021/AC071528Q. URL: /pmc/articles/PMC2435225/%20/pmc/articles/PMC2435225/?report=abstract%20https://www.ncbi.nlm.nih.gov/pmc/articles/PMC2435225/.

- [87] Sumedh P. Surwade, Sergei N. Smirnov, Ivan V. Vlassiouk, et al. “Water desalination using nanoporous single-layer graphene”. In: *Nature Nanotechnology* 2015 10:5 10.5 (Mar. 2015), pp. 459–464. ISSN: 1748-3395. DOI: 10.1038/nnano.2015.37. URL: <https://www.nature.com/articles/nnano.2015.37>.
- [88] Ali Ashraf, Yanbin Wu, Michael C. Wang, et al. “Spectroscopic investigation of the wettability of multilayer graphene using highly ordered pyrolytic graphite as a model material”. In: *Langmuir* 30.43 (Nov. 2014), pp. 12827–12836. ISSN: 15205827. DOI: 10.1021/LA503089K/SUPPL_FILE/LA503089K_SI_001.PDF. URL: <https://pubs.acs.org/doi/full/10.1021/la503089k>.
- [89] Grzegorz Stando, Damian Łukawski, Filip Lisiecki, et al. “Intrinsic hydrophilic character of carbon nanotube networks”. In: *Applied Surface Science* 463 (Jan. 2019), pp. 227–233. ISSN: 0169-4332. DOI: 10.1016/J.APSUSC.2018.08.206.
- [90] Minsuk Park, In Seung Choi, and Sang Yong Ju. “Quantification and removal of carbonaceous impurities in a surfactant-assisted carbon nanotube dispersion and its implication on electronic properties”. In: *Nanoscale Advances* 4.17 (Aug. 2022), pp. 3537–3548. ISSN: 2516-0230. DOI: 10.1039/D2NA00153E. URL: <https://pubs.rsc.org/en/content/articlehtml/2022/na/d2na00153e%20https://pubs.rsc.org/en/content/articlelanding/2022/na/d2na00153e>.
- [91] Young Jun Shin, Yingying Wang, Han Huang, et al. “Surface-energy engineering of graphene”. In: *Langmuir* 26.6 (Mar. 2010), pp. 3798–3802. ISSN: 07437463. DOI: 10.1021/LA100231U/ASSET/IMAGES/LARGE/LA-2010-00231U_0005.JPG. URL: <https://pubs.acs.org/doi/full/10.1021/la100231u>.
- [92] Creative PEGWorks. *Functionalisation with Pyrene-PEG-Rhodamine*. 2022.
- [93] Robert D. Deegan, Olgica Bakajin, Todd F. Dupont, et al. “Capillary flow as the cause of ring stains from dried liquid drops”. In: *Nature* 1997 389:6653 389.6653 (1997), pp. 827–829. ISSN: 1476-4687. DOI: 10.1038/39827. URL: <https://www.nature.com/articles/39827>.
- [94] Shunsuke F. Shimobayashi, Mikiko Tsudome, and Tomo Kurimura. “Suppression of the coffee-ring effect by sugar-assisted depinning of contact line”. In: *Scientific Reports* 2018 8:1 8.1 (Dec. 2018), pp. 1–9. ISSN: 2045-2322. DOI: 10.1038/s41598-018-35998-w. URL: <https://www.nature.com/articles/s41598-018-35998-w>.
- [95] David C. Stone. “Application of median filtering to noisy data”. In: 73.10 (Oct. 2011), pp. 1573–1581. ISSN: 0008-4042. DOI: 10.1139/V95-195. URL: <https://cdnsciencepub.com/doi/10.1139/v95-195>.